Eur. Phys. J. C (2017) 77:125
DOI 10.1140/epjc/s10052-017-4685-0

THE EUROPEAN PHYSICAL JOURNAL C

Regular Article - Theoretical Physics

Analysis of charmless two-body B decays in factorization-assisted topological-amplitude approach

Si-Hong Zhou[1,2,a], **Qi-An Zhang**[1,2], **Wei-Ran Lyu**[3], **Cai-Dian Lü**[1,2]

[1] Institute of High Energy Physics, YuQuanLu 19B, Beijing 100049, China
[2] School of Physics, University of Chinese Academy of Sciences, YuQuanLu 19A, Beijing 100049, China
[3] Physics Department, Renmin University of China, ZhongGuanCun St. 59, Beijing 100872, China

Received: 20 October 2016 / Accepted: 8 February 2017 / Published online: 23 February 2017

Abstract We analyze charmless two-body non-leptonic B decays $B \to PP, PV$ under the framework of a factorization-assisted topological-amplitude approach, where $P(V)$ denotes a light pseudoscalar (vector) meson. Compared with the conventional flavor diagram approach, we consider the flavor $SU(3)$ breaking effect assisted by a factorization hypothesis for topological diagram amplitudes of different decay modes, factorizing out the corresponding decay constants and form factors. The non-perturbative parameters of topology diagram magnitudes χ and the strong phase ϕ are universal; they can be extracted by χ^2 fit from current abundant experimental data of charmless Bdecays. The number of free parameters and the χ^2 per degree of freedom are both reduced compared with previous analyses. With these best fitted parameters, we predict branching fractions and CP asymmetry parameters of nearly 100 $B_{u,d}$ and B_s decay modes. The long-standing $\pi\pi$ and πK-CP puzzles are solved simultaneously.

1 Introduction

Charmless two-body non-leptonic B decays are of importance for testing the standard model (SM). They can be used to study CP violation via the interference of tree and penguin contributions. They are also sensitive to signals of new physics that would change the small loop effects from penguin diagrams. With regard to them, the BaBar and Bell experiments at the e^+e^- B-factories [1] and LHCb experiment at the large hadron collider (LHC) [2] have made great efforts in studying B decays information in the past decades. Numerous data of branching fractions and CP asymmetries of $B \to PP, PV$ decays, where $P(V)$ denotes a light pseudoscalar (vector) meson, have been measured. In particular, running at higher sensitivities and statistics, several B_s decay channels have been observed in the LHCb experiment. Such abundant experimental data have made it possible to extract non-perturbative parameters of hadronic decay amplitudes and to test theoretical calculations of the $B \to PP, PV$ decays.

On the theoretical side, as the non-leptonic Bdecays include hadronic decay amplitudes, it requires complicated study of non-perturbative strong QCD dynamics. Furthermore, the charmless B decays not only involve tree topologies but also have penguin loop diagrams that made the theoretical calculations more complex. The measured large direct CP violation in charmless B decays indicates the existence of large strong phases, which mainly come from non-perturbative QCD dynamics. In the heavy b quark mass limit, we can factorize the perturbative calculable part from the non-perturbative hadronic matrix elements. The naive factorization approach [3] was first invented to estimate the hadronic decay amplitudes, where they were factorized into the product of perturbative hard kernels (local four-quark operators) and non-perturbative objects such as B to light form factors and decay constants of light pseudoscalar/vector mesons. Then it was later improved to the generalized factorization approach [4,5]. Based on the leading-order power expansion of $\Lambda_{\rm QCD}/m_b$, where $\Lambda_{\rm QCD}$ represents the typical non-perturbative QCD hadronic scale, m_b is b quark mass, the QCD factorization (QCDF) [6], the perturbative QCD (PQCD) [7,8], and the soft-collinear effective theory (SCET) [9] have been developed recently. Great theoretical progress has been made in these perturbative QCD approaches. However, it is impossible to calculate to all orders of power expansions, thus some strong QCD dynamics information would be lost in these perturbative approaches. With the very high precision of experimental data, the leading-order theoretical calculation of the $\Lambda_{\rm QCD}/m_b$ expansion is not enough. For example, the QCDF [10] needs to include a

[a] e-mail: shzhou@ihep.ac.cn

large penguin annihilation contribution (as free parameter) to enhance the branching fractions and direct *CP* asymmetry of penguin-dominated charmless B decays. The same puzzle also appeared in SCET [11], where the penguin annihilation contribution in the QCDF is replaced by the power suppressed non-perturbative charming penguin effect (but with larger numerical contribution than the leading terms). All these power corrections cannot be calculated perturbatively but need to be fitted from experiments. There are also some experimental puzzles to be solved for those perturbative approaches. The perturbative calculation predicts the same sign of direct *CP* asymmetry in $B^{\pm} \to \pi^0 K^{\pm}$ and in $B^0 \to \pi^{\mp} K^{\pm}$ decays, which is in conflict with experimental data. The calculated branching ratio of $B^0 \to \pi^0\pi^0$ in perturbative approaches is several times smaller than the measured one. These long-standing puzzles are sensitive to the non-factorizable color-suppressed emission diagram. Although some soft and sub-leading effects were taken into account in the QCDF [10] and the PQCD [12], the $B \to \pi\pi$ puzzle was still left in the conventional factorization theorem. Recently, an additional Glauber phase was introduced to solve this puzzle [13].

Unlike the above mentioned perturbative approaches, some model-independent approaches were introduced to analyze the charmless B decays, such as global $SU(3)/U(3)$ flavor symmetry analysis [14] and flavor topological diagram approach [15–17]. They do not apply factorization in QCD, leaving all perturbative or non-perturbative QCD effects extracted from experimental data. In [14], one related relevant decay amplitudes using a $SU(3)/U(3)$ group decomposition and then extracted them from the experimental data. For the flavor topological diagram approach, they group different contributions according to the electroweak topological diagram, since electroweak interaction naturally factorize from QCD interaction. Each topological diagram amplitude including all strong interactions with strong phase are to be extracted from experimental data. However, in order to reduce the number of free parameters, one needs to apply the flavor $SU(3)$ symmetry to relate topological diagram parameters of different decay modes. In fact, the flavor $SU(3)$ symmetry is broken. Nowadays, $SU(3)$ breaking effects have to be considered to compare the theoretical results with the precise experimental data. It is also observed in the flavor topological diagram analysis that there are large differences among the three types of $B \to PP$, $B \to PV$ and $B \to VP$ decays due to different pseudoscalar and vector final states. Therefore, they have to fit three different sets of parameters for the three types of B decays, respectively [17]. There are too many parameters to be fitted; its prediction power was reduced.

In view of the above complexity and incompleteness in power correction of factorization approaches and the limitation of the conventional flavor topological diagram approach, a new method called a factorization-assisted topological-amplitude (FAT) approach was proposed in studying the two-body hadronic decays of D mesons [18,19]. Aiming to include all non-factorizable/non-perturbative QCD contributions, to be compared to factorization approaches, it adopts the formalism of a flavor topological diagram approach. However, different from the conventional flavor topological diagram approach, it had included $SU(3)$ breaking effect in each flavor topological diagram assisted by a factorization hypothesis. The FAT approach applied in D mesons decays [18,19] had great success to resolve the long-standing puzzle from the large difference of $D^0 \to \pi^+\pi^-$ and $D^0 \to K^+K^-$ branching fractions, due to large $SU(3)$ breaking effects. It also predicted 0.1% of the direct CP asymmetry difference between these two decay channels, later confirmed by the LHCb experiment [20,21]. With an intermediate charm quark scale, the two-body charmed meson decays of the B meson also encounter large $SU(3)$ breaking effects [22]. With only four parameters fitted from 31 experimental observations, we predict 120 decay modes, some of which are tested by the available experimental data [22].

In this work, we will analyze the charmless $B \to PP, PV$ decays in the FAT approach. Being different from the two-body charmed B meson decays with only tree diagrams, penguin diagrams enhanced by CKM matrix elements will contribute to these charmless B meson decays. These loop effects will be more complicated than the calculation of tree level diagrams. More theoretical parameters are needed to describe these penguin topological amplitudes and more experimental observables, such as *CP* asymmetry parameters. Specifically, including penguin topological contributions, we will fit 14 parameters from 37 experimental measured branching fractions and 11 *CP* asymmetry parameters of $B \to PP$ and $B \to PV$ decays. The number of free parameters is significantly reduced from the previous topological diagram approach with much less χ^2 per degree of freedom. The long-standing $B \to \pi\pi$ puzzle and $B \to \pi K$ *CP* puzzle are resolved consistently.

In Sect. 2, we parameterize the tree and penguin topological amplitudes of charmless $B \to PP$, PV decays in the FAT approach. The numerical results and discussions are presented in Sect. 3. Section 4 is the conclusion.

2 Factorization of decay amplitudes for different topological diagrams

The two-body charmless B decays are flavor changing weak decays. They are induced by the quark level diagrams classified by leading-order (tree diagram) and 1-loop level (penguin diagram) weak interactions. For different B decay final states, the tree level weak decay diagram can contribute via different orientations: the so-called color-favored tree emis-

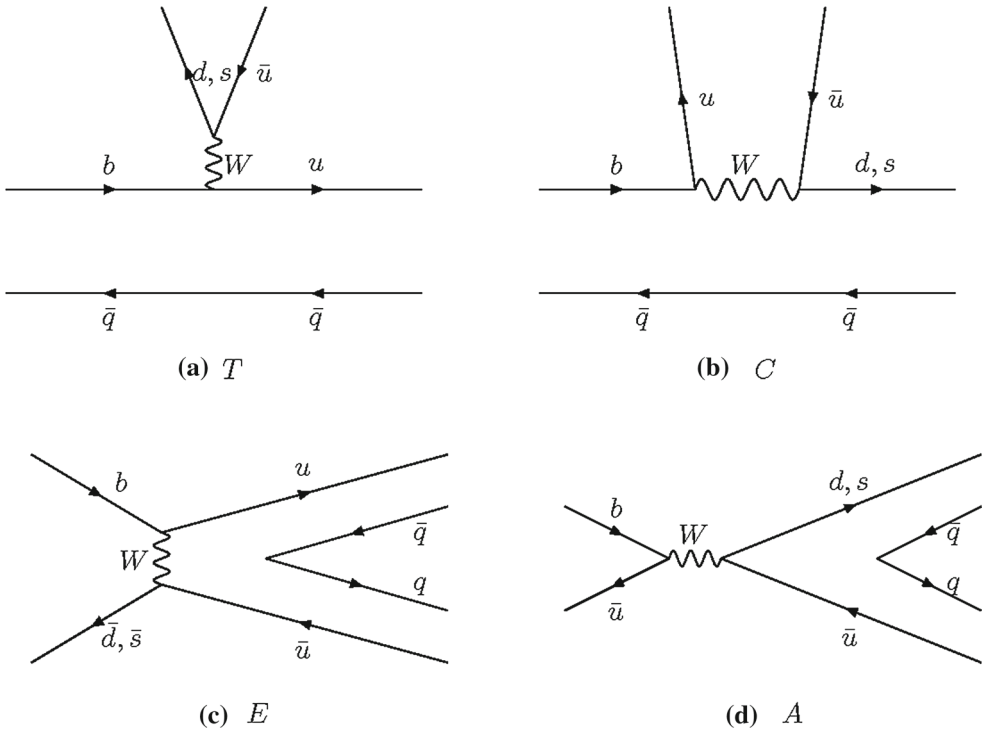

Fig. 1 Topological tree diagrams contributing to $B \to PP$ and $B \to PV$ decays: **a** the color-favored tree emission diagram, T; **b** the color-suppressed tree emission diagram, C; **c** the W-exchange diagram, E and **d** the W-annihilation diagram, A

sion diagram T, color-suppressed tree emission diagram C, W-exchange tree diagrams E and W annihilation tree diagrams A, which are shown in Fig. 1, respectively. These tree level diagrams have already been studied in the previous D meson decays [18,19] and charmed meson final state B decays [22]. Similarly, the 1-loop penguin diagram can also be classified into five types: color-favored QCD-penguin emission diagram P, color-suppressed QCD-penguin emission diagram P_C, W-annihilation penguin diagram P_A, the W penguin-exchange diagram P_E, and the electroweak penguin emission diagram P_{EW}, shown in Fig. 2.

The QCD factorization can be proved only at leading order of a $1/m_b$ expansion in most cases. Although the QCDF approach gives successful results in the leading order of $1/m_b$ expansion, it fails in many channels with big sub-leading contributions, compared with precision experimental data, such as the famous $K\pi$ puzzle. Ciuchini et al. [23] use the QCD factorization approach to calculate the leading-order contribution in a $1/m_b$ expansion of $B \to \pi K$ modes; while for the non-accurate sub-leading terms in the $1/m_b$ expansion, they fit them from the experimental data. The $K\pi$ puzzle is then explained. Our FAT approach modified from the conventional diagrammatic approach is equivalent to the one in [23], but we have an extension to all charmless $B \to PP$, PV, and VP modes. In the conventional topological diagram approach [17], one has to assume the flavor $SU(3)$ symmetry, reducing the number of independent parameters, in order to have predictive power. The precision of this topological diagram approach is then limited to the order of $SU(3)$ breaking. In the FAT approach, we will try to recover the $SU(3)$ breaking effects, further reducing the number of free parameters by fitting all the decay channels.

Let us start from tree amplitudes shown in Fig. 1. In the conventional topological diagram approach, the color-favored tree amplitude (T) is tuned to be a real number, with six parameters (magnitudes and phases) for three other amplitudes. However, these seven parameters have to be tripled for $B \to PP$, $B \to PV$, and $B \to VP$ decays, since there is a non-negligible difference between pseudoscalar and vector mesons. In this work, we will try to parametrize these three kinds of decays together. The color-favored T topology shown in Fig. 1a is proved factorization to all orders of α_s expansion in QCD factorization approaches and SCET. Their numerical results also agree to each other in different approaches. Thus, to reduce one free parameter, we will just use their theoretical results, not fitting from the experiments:

$$\begin{aligned} T^{P_1P_2} &= i\frac{G_F}{\sqrt{2}}V_{ub}V_{uq'}a_1(\mu)f_{p_2}(m_B^2 - m_{p_1}^2)F_0^{BP_1}(m_{p_2}^2), \\ T^{PV} &= \sqrt{2}G_F V_{ub}V_{uq'}a_1(\mu)f_V m_V F_1^{B-P}(m_V^2)(\varepsilon_V^* \cdot p_B), \\ T^{VP} &= \sqrt{2}G_F V_{ub}V_{uq'}a_1(\mu)f_P m_V A_0^{B-V}(m_P^2)(\varepsilon_V^* \cdot p_B), \end{aligned} \tag{1}$$

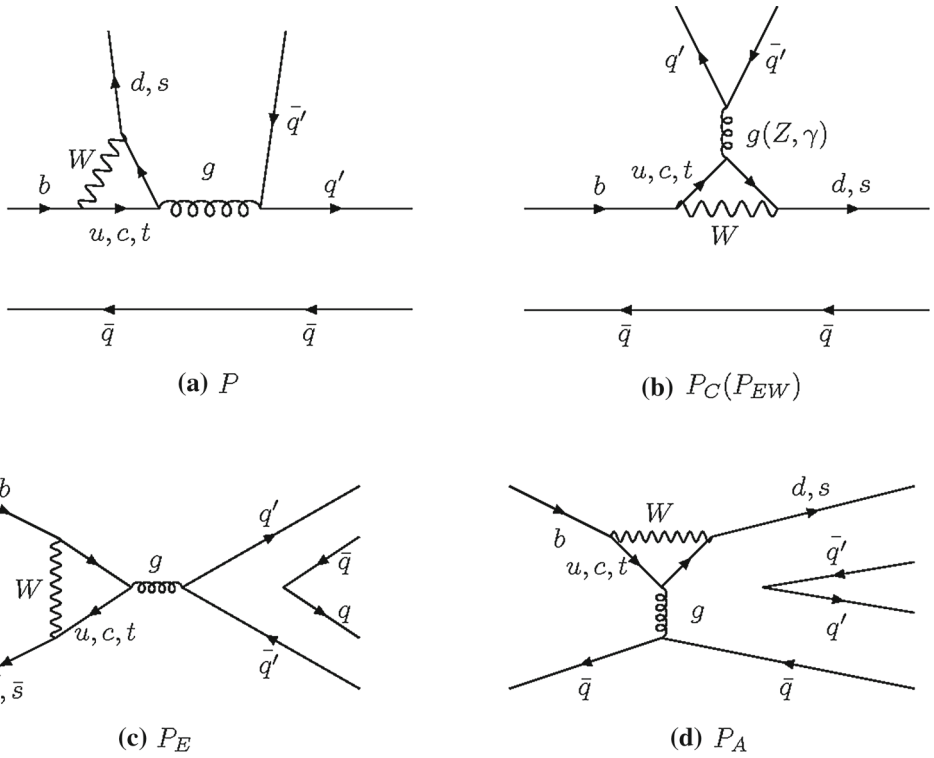

Fig. 2 Topological penguin diagrams contributing to $B \to PP$ and $B \to PV$ decays: **a** the color-favored QCD-penguin diagram, P; **b** the flavor-singlet QCD-penguin diagram, P_C, and EW-penguin diagram, P_{EW}; **c** the exchange type QCD-penguin diagram, P_E, and **d** the QCD-penguin annihilation diagram, P_A

where the superscript of $T^{P_1P_2}$ denotes the final mesons, two pseudoscalar mesons, $T^{PV(VP)}$ for recoiling mesons are a pseudoscalar meson (vector meson). $a_1(\mu)$ is the effective Wilson coefficient from short-distance QCD corrections, where the factorization scale μ is insensitive to different final state mesons. Therefore we can choose it within a certain range arbitrarily and set it at the point $\mu = m_b/2 = 2.1$ GeV. By now there are already NNLO QCD calculations available for Wilson coefficient a_1 [24], even including a phase. However, the NNLO results give very small numerical corrections comparing with the NLO results. Furthermore, there are no NNLO calculations to other Wilson coefficients. To be consistent, the Wilson coefficients we used in this paper are all at next-to-leading order (NLO) $a_1(\mu) = C_2(\mu) + C_1(\mu)/3 = 1.05$ [12]. $f_{P_2}(f_P)$ and f_V are the decay constants of the emitted pseudoscalar meson and vector meson, respectively. $F_0^{BP_1}$ (F_1^{B-P}) and A_0^{B-V} are the form factors of $B \to P$ and $B \to V$ transitions, respectively. ε_V^* is the polarization vector of the vector meson and p_B is the 4-momentum of the B meson.

As for the color-suppressed C topology, dominated by non-factorization contributions: it is least understood by us although having been calculated up to next-to-leading order in the factorization methods. The next-to-leading order corrections in factorization framework could not resolve the $\pi\pi$ and πK puzzles strongly sensitive to this C topology contribution. A large C contribution with a large strong phase (mostly non-perturbative) can resolve the so-called πK puzzle. However, it is not possible to explain the $\pi\pi$ puzzle: theoretically $Br(B^0 \to \pi^0\pi^0) < Br(B^0 \to \pi^0\rho^0) < Br(B^0 \to \rho^0\rho^0)$, but experimentally it is in the inverse order. In the conventional topological diagram approach [17], the authors introduced two parameters (amplitude and phase) in the $B \to PP$ modes and another four parameters in the $B \to PV$, VP modes for this diagram to be fitted from experimental data. To the best of our knowledge, this inverse order can be understood only in the formalism of Glauber gluons introduced in [13], where an extra phase was introduced for the pseudoscalar meson (Goldstone boson) emission diagram. Inspired by these studies, we parameterize the C diagram magnitude and the associated phase as χ^C and $e^{i\phi^C}$ in $B \to PP$, VP decays, and $\chi^{C'}e^{i\phi^{C'}}$ in $B \to PV$, respectively, to distinguish cases in which the emitted meson is pseudoscalar or vector:

$$
\begin{aligned}
C^{P_1P_2} &= i\frac{G_F}{\sqrt{2}}V_{ub}V_{uq'}\chi^C e^{i\phi^C} f_{p_2}(m_B^2 - m_{p_1}^2)F_0^{BP_1}(m_{p_2}^2),\\
C^{PV} &= \sqrt{2}G_F V_{ub}V_{uq'}\chi^{C'}e^{i\phi^{C'}} f_V m_V F_1^{B-P}(m_V^2)(\varepsilon_V^* \cdot p_B),\\
C^{VP} &= \sqrt{2}G_F V_{ub}V_{uq'}\chi^C e^{i\phi^C} f_P m_V A_0^{B-V}(m_P^2)(\varepsilon_V^* \cdot p_B),
\end{aligned}
\tag{2}
$$

where the decay constants and form factors f_P, f_V, $F_0^{BP_1}$, F_1^{B-P} and A_0^{B-V} characterizing the $SU(3)$ breaking effects are factorized out.

The W-exchange E topology is non-factorization in QCD factorization approach. It is expected to be smaller than the emission diagram due to helicity suppression. We use χ^E, $e^{i\phi^E}$ to represent the magnitude and its strong phase for all decay modes:

$$\begin{aligned} E^{P_1P_2} &= i\frac{G_F}{\sqrt{2}}V_{ub}V_{uq'}\chi^E e^{i\phi^E} f_B m_B^2 \left(\frac{f_{p_1}f_{p_2}}{f_\pi^2}\right), \\ E^{PV,VP} &= \sqrt{2}G_F V_{ub}V_{uq'}\chi^E e^{i\phi^E} f_B m_V \left(\frac{f_P f_V}{f_\pi^2}\right) \\ &\quad \times (\varepsilon_V^* \cdot p_B). \end{aligned} \tag{3}$$

Considering flavor $SU(3)$ breaking effects, we multiply decay constants of three mesons f_B, $f_{p_1}(f_P)$, and $f_{p_2}(f_V)$ in each amplitude. In order to make parameters χ^E and $e^{i\phi^E}$ dimensionless, a normalization factor f_π^2 is introduced. Actually, the dimensionless parameters χ^E, $e^{i\phi^E}$ are defined from $B \to \pi\pi$ decays. Other processes are related by different decay constant factors $\frac{f_{p_2}f_{p_1}(f_P f_V)}{f_\pi f_\pi}$. The last diagram in Fig. 1d is the so-called W-annihilation topology. As discussed in Ref. [17], its contribution is negligible. We will also ignore it in this paper.

The penguin topological diagrams are grouped into QCD-penguin and electroweak penguin (EW penguin) topologies. In terms of QCD-penguin diagram amplitude, we consider all contributions from every topological diagram in Fig. 2, where topology P contributes most. The leading contribution from the topology P diagram is similar to the color-favored tree diagram T, which is a proved factorization in various QCD-inspired approaches, such as QCD factorization [10], perturbative QCD [7,8], and soft-collinear effective theory [25]. They give very similar numerical results proportional to the Wilson coefficient a_4, related to the QCD-penguin operators O_3, O_4. The NLO Wilson coefficient $a_4(\mu = 2.1) = -0.044$ and the quark-loop corrections and the magnetic-penguin contribution are also absorbed into the Wilson coefficient a_4 as in [12]. Therefore, in the same spirit of the T diagram, we will not fit this contribution from the experimental data, but predict its contribution from QCD calculations for all the three type of $B \to PP$, $B \to VP$ and $B \to PV$ decays. This is not the whole story. All these approaches predict a large extra contribution in this topology related to the effective four-quark operators O_5, O_6, also called the "chiral enhanced" penguin contributions. Since this chiral enhancement only contributes to the pseudoscalar meson (Goldstone boson) emission diagram, we will include it only in $B \to PP$ and $B \to VP$ decays, which can be parameterized as $r_\chi \chi^P$, $e^{i\phi^P}$ in Eq. (4) with r_χ the chiral factor of the pseudoscalar meson. The decay amplitude for the penguin diagram P is then parameterized with only two free parameters for all the three categories of $B \to PP$, $B \to VP$, and $B \to PV$ decays, thus

$$\begin{aligned} P^{PP} &= -i\frac{G_F}{\sqrt{2}}V_{tb}V_{tq'}^*\left[a_4(\mu) + \chi^P e^{i\phi^P} r_\chi\right] \\ &\quad \times f_{p_2}(m_B^2 - m_{p_1}^2)F_0^{BP_1}(m_{p_2}^2), \\ P^{PV} &= -\sqrt{2}G_F V_{tb}V_{tq'}^* a_4(\mu) f_V m_V F_1^{B-P} m_V^2 (\varepsilon_V^* \cdot p_B), \\ P^{VP} &= -\sqrt{2}G_F V_{tb}V_{tq'}^*\left[a_4(\mu) - \chi^P e^{i\phi^P} r_\chi\right] \\ &\quad \times f_P m_V A_0^{B-V}(m_P^2)(\varepsilon_V^* \cdot p_B). \end{aligned} \tag{4}$$

The so-called penguin annihilation diagram P_A shown in Fig. 2d was considered as a power correction to P, calculated perturbatively in PQCD approach [7,8], parameterized as ρ_A, ϕ_A in QCDF [10] and replaced by the long-distance charm penguins as A_{cc}^{PP}, A_{cc}^{PV}, and A_{cc}^{VP} in $B \to PP$, $B \to VP$ and $B \to PV$ decays, respectively, in SCET [25]. Numerically it is not small. However, if one examines this diagram carefully, one can find that it is not distinguishable in the weak interaction from the diagram P in Fig. 2a. The only difference between these two diagrams is the gluon exchange. Since all the QCD dynamics will be determined by χ^2 fit from the experimental data, we will not introduce more parameters for this diagram in $B \to PP$ and $B \to VP$ decays. The contribution of this diagram is already encoded in the parameter $r_\chi \chi^P$, $e^{i\phi^P}$ in Eq. (4) for diagram Fig. 2a. But for $B \to PV$ decays, we do need two parameters χ^{P_A}, $e^{i\phi^{P_A}}$ for the penguin annihilation diagram P_A shown in Fig. 2d:

$$\begin{aligned} P_A^{PV} &= -\sqrt{2}G_F V_{tb}V_{tq'}^* \chi^{P_A} e^{i\phi^{P_A}} f_B m_V \left(\frac{f_P f_V}{f_\pi^2}\right) \\ &\quad \times (\varepsilon_V^* \cdot p_B). \end{aligned} \tag{5}$$

The contribution from the P_E diagram shown in Fig. 2c is argued to be smaller than the P_A diagram, which can be ignored reliably in decay modes not dominated by it such as measured $B^0 \to \pi^+\pi^-$, $B^0 \to \pi^0\pi^0$, $B^0 \to K^0\bar{K}^0$ and $B^0 \to \pi^0\rho^0$ decays. This P_E contribution actually is the dominant contribution for the recent measurement of $B_s \to \pi^+\pi^-$ decay [26]

$$Br(B_s \to \pi^+\pi^-) = (0.76 \pm 0.19) \times 10^{-6}.$$

We do not intend to use this single measurement to determine the contribution from this diagram P_E. Thus we have to ignore it for later discussion.

The flavor-singlet QCD-penguin diagram P_C only contribute to the isospin singlet mesons η, η', ω and ϕ. Anomaly related or not, there is also a significant difference between these pseudoscalar mesons and vector mesons. We distin-

guish them as χ^{P_C}, $e^{i\phi^{P_C}}$ for $B \to PP$ and $B \to VP$ decays and $\chi^{P'_C}$, $e^{i\phi^{P'_C}}$ for $B \to PV$ decays, respectively:

$$\begin{aligned} P_C^{PP} &= -i\frac{G_F}{\sqrt{2}} V_{tb}V_{tq'}^* \chi^{P_C} e^{i\phi^{P_C}} f_{p_2}(m_B^2 - m_{p_1}^2) F_0^{BP_1}(m_{p_2}^2), \\ P_C^{PV} &= -\sqrt{2} G_F V_{tb}V_{tq'}^* \chi^{P'_C} e^{i\phi^{P'_C}} f_V m_V F_1^{B-P}(m_V^2)(\varepsilon_V^* \cdot p_B), \\ P_C^{VP} &= -\sqrt{2} G_F V_{tb}V_{tq'}^* \chi^{P_C} e^{i\phi^{P_C}} f_P m_V A_0^{B-V}(m_P^2)(\varepsilon_V^* \cdot p_B). \end{aligned} \tag{6}$$

The EW-penguin contribution is much smaller than the QCD-penguin diagram, as the coupling coefficient α is one order smaller than α_s. We only keep its largest contribution diagram shown in the second one of Fig. 2, with gluon g replaced by Z or γ with respect to the QCD-penguin diagram. Although the topology of P_C diagram is quite similar to the P_{EW} topology, their contributions are different. They both contribute to the isospin singlet meson emission decays. But the P_{EW} topology also contributes to the neutral isospin 1 meson emission decays. The topology of this diagram is very similar to the T diagram. Factorization can be approved without ambiguity. Without introducing new parameters, we evaluate it similar to T,

$$\begin{aligned} P_{EW}^{PP} &= -i\frac{G_F}{\sqrt{2}} V_{tb}V_{tq'}^* e_q \frac{3}{2} a_9(\mu) f_{p_2}(m_B^2 - m_{p_1}^2) F_0^{BP_1}(m_{p_2}^2), \\ P_{EW}^{PV} &= -\sqrt{2} G_F V_{tb}V_{tq'}^* e_q \frac{3}{2} a_9(\mu) f_V m_V F_1^{B-P}(m_V^2)(\varepsilon_V^* \cdot p_B), \\ P_{EW}^{VP} &= -\sqrt{2} G_F V_{tb}V_{tq'}^* e_q \frac{3}{2} a_9(\mu) f_P m_V A_0^{B-V}(m_P^2)(\varepsilon_V^* \cdot p_B), \end{aligned} \tag{7}$$

where $a_9(\mu)$ is the NLO effective Wilson coefficient equal to -0.009 at scale $\mu = 2.1$ GeV.

In all, after the usage of the factorization theorem, the number of theoretical parameters to be fitted from experimental data is reduced. The six parameters for the tree diagrams are: color-suppressed tree diagram amplitude χ^C, $\chi^{C'}$ and their phases ϕ^C, $\phi^{C'}$; W-exchange diagram amplitude χ^E and its phase ϕ^E. The eight parameters for the penguin diagrams are: chiral enhanced penguin amplitude χ^P and its phase ϕ^P; flavor-singlet penguin amplitude χ^{P_C}, $\chi^{P'_C}$ and their phases ϕ^{P_C}, $\phi^{P'_C}$ for the pseudoscalar and vector meson emission, respectively; the penguin annihilation amplitude χ^{P_A} and its phase ϕ^{P_A} for the vector meson emission only. The mapping of these topologies to the well-known QCDF amplitudes introduced in [27], their numerical results for πK modes calculated in [28], is shown in Table 1.

The decay amplitude of each charmless B decay mode constituted by the above various topological amplitudes. The explicit contributions for each mode will be shown in the tables of Sect. 3.3. But remember that the topological amplitudes are summed with pre-factors of $1, -1, \pm 1/\sqrt{2}, \cos\phi, \sin\phi$ for the sake of isospin and flavor mixing. For example, the amplitude for $B^- \to \pi^-\eta$ can be written as

$$\begin{aligned} A_{\pi^-\eta} = &\frac{\cos\phi}{\sqrt{2}}(T + C + P) \\ &+ \left(\frac{2\cos\phi}{\sqrt{2}} - \frac{\sin\phi}{\sqrt{2}}\right)(P_C + P_{EW}), \end{aligned} \tag{8}$$

where T, C, P, P_C, and P_{EW} are topological amplitudes in formulas (1–7) and ϕ is the η–η' mixing angle introduced in Eq. (17) specifically. The decay width for two-body charmless B decays is given by

$$\Gamma(B \to M_1 M_2) = \frac{p}{8\pi m_B^2} \sum_{\text{pol}} |\mathcal{A}|^2, \tag{9}$$

where M_1, M_2 represent either two pseudoscalar P_1, P_2 or one pseudoscalar P and one vector V in the final states. p is the 3-dimension momentum of either meson in the final state in the center-of-mass frame. The summation over the polarization states is for vector meson state. The corresponding branching fraction is

$$\mathcal{B}(B \to M_1 M_2) = \frac{\Gamma(B \to M_1 M_2) + \Gamma(\bar{B} \to \bar{M}_1 \bar{M}_2)}{2} \times \tau_B, \tag{10}$$

where τ_B is the B meson lifetime. The CP violation charge asymmetry of exclusive B^- and B^+ decay is defined as

$$\mathcal{A}_{cp} = \frac{\mathcal{B}(B^- \to \bar{M}_1 \bar{M}_2) - \mathcal{B}(B^+ \to M_1 M_2)}{\mathcal{B}(B^- \to \bar{M}_1 \bar{M}_2) + \mathcal{B}(B^+ \to M_1 M_2)}. \tag{11}$$

For the neutral $B_{(s)}$ mesons, there is a complication because of the $B^0_{(s)}$–$\overline{B}^0_{(s)}$ mixing, if the decay product is a CP eigenstate. The CP asymmetry is time dependent:

$$\mathcal{A}_{cp}(t) = \mathcal{S}_f \sin(\Delta m_B t) - \mathcal{C}_f \cos(\Delta m_B t), \tag{12}$$

where Δm_B is the mass difference between the two mass eigenvalues of B mesons. $\mathcal{A}_{cp} \equiv -\mathcal{C}_f$ is the direct CP asymmetry and $\mathcal{S}_f$ is the mixing-induced CP asymmetry parameter, which are calculated to be

$$\begin{aligned} \mathcal{C}_f &= \frac{1 - |\lambda_f|^2}{1 + |\lambda_f|^2}, \\ \mathcal{S}_f &= \frac{2Im(\lambda_f)}{1 + |\lambda_f|^2}, \end{aligned} \tag{13}$$

where $\lambda_f = \frac{q}{p}\frac{\bar{A}_f}{A_f}$ and $\frac{q}{p} = \frac{V_{tb}^* V_{td}}{V_{tb} V_{td}^*}$ or $\left(\frac{V_{tb}^* V_{ts}}{V_{tb} V_{ts}^*}\right)$, which is the mixing parameter for $B^0_{(s)}$–$\overline{B}^0_{(s)}$ mixing. A_f is the decay amplitude of $B^0 \to f_{CP}$ and $\bar{A}_f$ is the amplitude of the CP-conjugate process.

Table 1 The amplitudes and strong phases of topological diagrams in the FAT corresponding to contributions in the QCDF. The topology A and P_E are neglected in the FAT. The electroweak penguin contributions of $\alpha_4^{\rm EW}$, $\beta_3^{\rm EW}$ and $\beta_4^{\rm EW}$ in the QCDF are also neglected in the FAT

Diagram	T	C	P_C	P(PP)	P_{EW}	E	A	P_A(PV)	P_E
FAT	a_1	$\chi^{C^{(\prime)}}e^{i\phi^{C^{(\prime)}}}$	$\chi^{P_C^{(\prime)}}e^{i\phi^{P_C^{(\prime)}}}$	$a_4(\mu)+\chi^P e^{i\phi^P} r_\chi$	$a_9(\mu)$	$\chi^E e^{i\phi^E}$	–	$-i\chi^{P_A}e^{i\phi^{P_A}}$	–
	–	$0.48e^{-1.58i}$	$0.048e^{1.56i}$	$-0.12e^{-0.24i}$	-0.009	$0.057e^{2.71i}$		$0.0059e^{-0.006i}$	
QCDF	α_1	α_2	α_3	α_4	$\alpha_3^{\rm EW}$	β_1	β_2	β_3	β_4
	–	$0.22e^{-0.53i}$	$0.011e^{2.23i}$	$-0.089e^{0.11i}$	$-0.009e^{0.04i}$	0.025	-0.011	-0.008	-0.003

If the decay product is not the CP eigenstate, the $B^0_{(s)}$–$\overline{B}^0_{(s)}$ mixing will not result in a mixing-induced CP asymmetry, but only a direct CP asymmetry like the $B^\pm$ decays (for example $B^0 \to \pi^- K^+$). However, for the $\bar{B}^0 \to \pi^\pm\rho^\mp$, $\bar{B}^0 \to K_s\bar{K}^{*0}(K^{*0})$, $\bar{B}_s \to K^\pm K^{*\mp}$, and $\bar{B}_s \to K_s\bar{K}^{*0}(K^{*0})$ decay modes, the $B^0_{(s)}$–$\overline{B}^0_{(s)}$ mixing still plays an important role, even if the final states are not CP eigenstates. The reason is that both the $B^0_{(s)}$ and the $\overline{B}^0_{(s)}$ meson can decay to the same final state. The CP asymmetry is time dependent with four equations [29]. There is a mismatch between theoretical and experimental variables. We adopt the convention of [17], for example, the mixing-induced CP asymmetries S_{CP} for the $\bar{B}^0 \to \pi^\pm\rho^\mp$:

$$\begin{aligned}\mathcal{S}_{\bar{B}^0\to\pi^+\rho^-} &= \frac{2Im(\lambda_{\bar{B}^0\to\pi^+\rho^-})}{1+|\lambda_{\bar{B}^0\to\pi^+\rho^-}|^2},\\ \mathcal{S}_{\bar{B}^0\to\pi^-\rho^+} &= \frac{2Im(\lambda_{\bar{B}^0\to\pi^-\rho^+})}{1+|\lambda_{\bar{B}^0\to\pi^-\rho^+}|^2},\end{aligned} \tag{14}$$

where

$$\begin{aligned}\lambda_{\bar{B}^0\to\pi^+\rho^-} &= \frac{q}{p}\frac{A(\bar{B}^0\to\pi^+\rho^-)}{A(B^0\to\pi^-\rho^+)},\\ \lambda_{\bar{B}^0\to\pi^-\rho^+} &= \frac{q}{p}\frac{A(\bar{B}^0\to\pi^-\rho^+)}{A(B^0\to\pi^+\rho^-)}.\end{aligned} \tag{15}$$

The definition of S_{cp} for the $\bar{B}^0 \to K_s\bar{K}^{*0}(K^{*0})$, $\bar{B}_s \to K^\pm K^{*\mp}$, and $\bar{B}_s \to K_s\bar{K}^{*0}(K^{*0})$ decays are similar to $\bar{B}^0 \to \pi^\pm\rho^\mp$.

3 Numerical results and discussions

3.1 Input parameters

The input parameters used in decay amplitudes mainly contain the CKM matrix elements, decay constants, and transition form factors. We use the Wolfenstein parametrization for V_{CKM} with the Wolfenstein parameters obtained from [26]:

$$\begin{aligned}&\lambda = 0.22537 \pm 0.00061, \quad A = 0.814^{+0.023}_{-0.024}\\ &\bar{\rho} = 0.117 \pm 0.021, \quad \bar{\eta} = 0.353 \pm 0.013.\end{aligned}$$

Table 2 The decay constants of light pseudoscalar mesons and vector mesons (in units of MeV)

f_π	f_K	f_B	f_{B_s}	f_ρ	f_{K^*}	f_ω	f_ϕ
130	156	190	225	213	220	192	225

Table 2 represents the decay constants of light meson (P, V). The measured f_π and f_K are given in average by PDG [26]. The value of f_B, f_{B_s} and the decay constants of vector mesons not measured directly in experiments but can be got from several theoretical approaches, such as in the covariant light front approach [30], light-cone sum rules [31,32], QCD sum rules [33–38], or lattice QCD [39–46]. We show only central values in Table 2 and keep 5% uncertainty, when we estimate the theoretical uncertainty of branching fractions and CP asymmetry parameters.

The transition form factors of B meson decays were calculated in various theoretical approaches, constitute quark model and light cone quark model [47–50], the covariant light front approach (LFQM) [30,51,52], light-cone sum rules [32,53–71], PQCD [72–80], and lattice QCD [81–83]. The central values of the transition form factors of B meson decays at $q^2 = 0$ are shown in Table 3. The error bar of them are kept in 10%. This uncertainty of the hadronic form factors is one of the major sources of theoretical uncertainty in our calculation as shown in the next section. For the q^2 dependence of the transition form factors, we use the dipole parametrization:

$$F_i(q^2) = \frac{F_i(0)}{1-\alpha_1\frac{q^2}{M^2_{\rm pole}}+\alpha_2\frac{q^4}{M^4_{\rm pole}}}, \tag{16}$$

where F_i denotes F_0, F_1, and A_0 in this article, and $M_{\rm pole}$ is the mass of the corresponding pole state, such as $B_{(s)}$ for A_0, and $B^*_{(s)}$ for $F_{0,1}$. The dipole parameters α_1 and α_2 shown in Table 3 are from [49,73]. Since the values of $q^2 = m^2_{P,V}$, where $m_{P,V}$ is the mass of the emission meson in $B \to PP$, PV decays, are small compared with the pole mass, this q^2 dependence will not affect our numerical results significantly.

Table 3 The transition form factors of B meson decays at $q^2 = 0$ and dipole model parameters

	$F_0^{B\to\pi}$	$F_0^{B\to K}$	$F_0^{B_s\to K}$	$F_0^{B\to\eta_q}$	$F_0^{B_s\to\eta_s}$
$F(0)$	0.28	0.31	0.25	0.21	0.30
α_1	0.50	0.53	0.54	0.52	0.53
α_2	−0.13	−0.13	−0.15	0	0
	$F_1^{B\to\pi}$	$F_1^{B\to K}$	$F_1^{B_s\to K}$	$F_1^{B\to\eta_q}$	$F_1^{B_s\to\eta_s}$
$F(0)$	0.28	0.31	0.25	0.21	0.30
α_1	0.52	0.54	0.57	1.43	1.48
α_2	0.45	0.50	0.50	0.41	0.46
	$A_0^{B\to\rho}$	$A_0^{B\to\omega}$	$A_0^{B\to K^*}$	$A_0^{B_s\to K^*}$	$A_0^{B_s\to\phi}$
$A(0)$	0.36	0.32	0.39	0.33	0.40
α_1	1.56	1.60	1.51	1.74	1.73
α_2	0.17	0.22	0.14	0.47	0.41

For the η and η' meson in the final state of B decays, their decay constants and form factors are defined through η–η' mixing,

$$\begin{pmatrix}\eta\\ \eta'\end{pmatrix} = \begin{pmatrix}\cos\phi & -\sin\phi\\ \sin\phi & \cos\phi\end{pmatrix}\begin{pmatrix}\eta_q\\ \eta_s\end{pmatrix}, \tag{17}$$

where η_q and η_s are defined by

$$\eta_q = \frac{1}{\sqrt{2}}(u\bar{u} + d\bar{d}), \quad \eta_s = s\bar{s}. \tag{18}$$

The mixing angle is measured to be $\phi = (40.4 \pm 0.6)^\circ$ by KLOE [84]. The flavor decay constants of η_q and η_s are $f_q = (1.07 \pm 0.02) f_\pi$ and $f_s = (1.34 \pm 0.06) f_\pi$, respectively [85,86]. In a good approximation, we neglect the ω and ϕ mixing effect.

3.2 The χ^2 fit for theoretical parameters

Many of the charmless B decays channels have been experimentally measured [26]. But some of them are measured with very poor precision. In our χ^2 fit program, we will not use those data with less than 3σ significance. For the B_s meson decays, very few modes are measured, some of which are measured only by hadronic colliders such LHCb and CDF experiments. The precision of these B_s decays measurements rely heavily on other B decay channels measured by B factories. Thus the systematic uncertainty of them is correlated. We will not use the B_s decay data to avoid complications. After these considerations, we have 37 branching ratios and 11 CP violation observations of $B_{u,d} \to PP, PV$ decays from the current experimental data, where the branching ratios of $B^0 \to \pi^+\rho^-$ and $B^0 \to \pi^-\rho^+$ are derived from experimental data in [17]. With these 48 data, we use the χ^2 fit method by Minuit program [87], where we have taken the input parameters including CKM, decay constants and form factors as fixed values shown in Sect. 3.1 and allow only 14 theoretical parameters to vary freely, to give the best-fitted parameters and the corresponding 1σ uncertainty:

$$\begin{aligned}
\chi^C &= 0.48 \pm 0.06, \quad \phi^C = -1.58 \pm 0.08,\\
\chi^{C'} &= 0.42 \pm 0.16, \quad \phi^{C'} = 1.59 \pm 0.17,\\
\chi^E &= 0.057 \pm 0.005, \quad \phi^E = 2.71 \pm 0.13,\\
\chi^P &= 0.10 \pm 0.02, \quad \phi^P = -0.61 \pm 0.02.\\
\chi^{P_C} &= 0.048 \pm 0.003, \quad \phi^{P_C} = 1.56 \pm 0.08,\\
\chi^{P'_C} &= 0.039 \pm 0.003, \quad \phi^{P'_C} = 0.68 \pm 0.08,\\
\chi^{P_A} &= 0.0059 \pm 0.0008, \quad \phi^{P_A} = 1.51 \pm 0.09,
\end{aligned} \tag{19}$$

with $\chi^2/\text{d.o.f} = 45.2/34 = 1.3$. This χ^2 per degree of freedom is smaller than the conventional flavor diagram approach based on flavor $SU(3)$ symmetry [17]. In fact, they have much more parameters [17] than in our work. From (19), one can see that the color-suppressed tree diagram amplitude χ^C and $\chi^{C'}$ have similar sizes but their phases ϕ^C and $\phi^{C'}$ differ significantly. Denoting the pseudoscalar and vector meson emission, respectively, their differences agree with the Glauber gluon effects [13]. Similar differences are observed in the flavor-singlet penguin amplitude χ^{P_C}, $\chi^{P'_C}$ and their phases ϕ^{P_C}, $\phi^{P'_C}$ for the pseudoscalar and vector meson emission, respectively. Since there is a one-to-one relation between the QCDF-amplitudes and topological diagrams, we show the different numerical values of these amplitudes in both approaches in Table 1. It is apparent that there are huge differences between numbers fitted from experimental data in the FAT and the calculated results in the QCDF, especially for the strong phases. Later we will show that the two small strong phases from perturbative QCD factorization contributions are the main reason for the $\pi\pi$ and πK puzzles.

To show the relative size of every topological diagram in each decay mode, we take decay modes $B \to \pi\pi$ and $B \to \pi\rho$ to show the hierarchy of various tree and penguin topologies amplitude ($C(P_C)$ and $C'(P'_C)$ denote the pseudoscalar and vector meson emission, respectively.), as follows:

$$T^{\pi\pi} : C^{\pi\pi} : E^{\pi\pi} : P^{\pi\pi} = 1 : 0.47 : 0.29 : 0.32 \tag{20}$$

$$T^{\rho\pi} : C^{\prime\pi\rho} : P^{\rho\pi} : P_{EW}^{\pi\rho} = 1 : 0.54 : 0.25 : 0.04 \tag{21}$$

$$T^{\pi\rho} : C^{\rho\pi} : P^{\rho\pi} : P_{EW}^{\rho\pi} = 1 : 0.36 : 0.19 : 0.03. \tag{22}$$

In these tree dominant decays, the relative importance of topological diagrams is easily seen:

$$T > C(C') > E \sim P > P_{EW}. \tag{23}$$

This is in agreement with those QCD-inspired approaches. For $B \to \pi K$ and $B \to \pi K^*$ decays, we have

$$T^{\pi K} : C^{\pi K} : P^{\pi K} : P_{EW}^{\pi K} = 1 : 0.4 : 6.0 : 0.6 \quad (24)$$

$$T^{\pi K^*} : C^{K^*\pi} : P^{\pi K^*} : P_A^{\pi K^*} : P_{EW}^{K^*\pi} = 1 : 0.37 : 2.87 : 1.44 : 0.52. \quad (25)$$

In these penguin-dominant decays, the relative importance of topological diagrams is also found:

$$P > P_A > T > P_{EW} > C. \quad (26)$$

It is interesting that the electroweak penguin contribution P_{EW} is even larger than the color-suppressed tree C. It is indeed not negligible. For $B \to \rho K$ decays, we have

$$T^{\rho K} : C'^{K\rho} : P^{\rho K} : P_{EW}^{K\rho} = 1 : 0.49 : 2.82 : 0.79. \quad (27)$$

In this channel, we have very similar contributions from each topology:

$$P > T > P_{EW} > C'. \quad (28)$$

Again, the electroweak penguin contribution P_{EW} is important.

As the P_C and P'_C only contribute to modes including flavor-singlet mesons (η, η', ω, ϕ), the hierarchies including P_C and P'_C are represented by

$$T^{\pi\eta} : C^{\pi\eta} : P^{\pi\eta} : P_C^{\pi\eta} : P_{EW}^{\pi\eta} = 1 : 0.50 : 0.57 : 0.06 : 0.03 \quad (29)$$

$$T^{\eta K} : C^{\eta K} : P^{\eta K} : P_C^{\eta K} : P_{EW}^{\eta K} = 1 : 0.45 : 3.39 : 1.10 : 0.52 \quad (30)$$

$$T^{\pi\omega} : C'^{\pi\omega} : P^{\pi\omega} : P_C'^{\pi\omega} : P_A^{\pi\omega} : P_{EW}^{\pi\omega} = 1 : 0.54 : 0.21 : 0.26 : 0.10 : 0.02. \quad (31)$$

The flavor-singlet penguin contribution P_C is important, as it is even larger than the color-favored tree contribution T in ηK channel and it is at a similar size to the penguin emission contribution P in $\pi\omega$ channel. The importance of this type of penguin contribution was recently emphasized [14].

3.3 Branching ratios for the charmless B decays

Using the parameters in (19), we get the numerical results of branching fractions for $\bar{B} \to PP$ decays shown in Table 4 and $\bar{B} \to PV$ decays in Table 5. All branching fraction tables are divided into two parts: $\Delta S = 0$ transitions and $\Delta S = 1$ transitions. Our results are well consistent with the experimental data or provide predictions to be tested in future experiments. We also show the contributing topological-amplitude symbols for each channel in these tables. For the theoretical uncertainties in the tables (applied also to the following tables), the first one is the statistical uncertainty from the χ^2 fitting by experimental data. The second one arises from the transition form factors which are set to be 10% uncertainties, and the third from decay constants. We can find that the dominant uncertainty for most channels is from the form factors, which need to be approved by theories and semi-leptonic B decay measurements. The experimental data are also shown in these tables to compare with theoretical predictions. Not all of the measurements have a good accuracy. In our χ^2 fit program, we use those data only with more than 3σ signal significance, marked $*$ in these tables. The rest can be considered as theoretical predictions, waiting for LHCb and other experiments to be tested.

From Tables 4 and 5, one can easily find that $\mathrm{B}(B^- \to \pi^-\pi^0)$ is twice smaller than $\mathrm{B}(B^- \to \pi^0\rho^-)$. These two modes receive similar contributions from the color-favored tree diagram denoted by T, while all other contributions are suppressed. If not considering $SU(3)$ breaking effects, one needs two parameters to fit these two diagrams in Ref. [17]. In our FAT approach, this can easily be explained by the fact that $f_\rho > f_\pi$, therefore we do not need any free parameter to be fitted from experimental data. Due to the difference between vector or pseudoscalar emission in the color-suppressed tree diagram $\chi^{C'}$ and χ^C, especially the very larger strong phase difference, the $\mathrm{B}(B^- \to \rho^-\pi^0)$ is a little different from $\mathrm{B}(B^- \to \rho^0\pi^-)$. Interestingly, for the penguin-dominated B decays we have the inverse situation. The branching fractions of the penguin diagram P dominated decay modes $B^- \to \pi^-\bar{K}^0$, $B^- \to \pi^0 K^-$, and $\bar{B}^0 \to \pi^0\bar{K}^0$ are larger than their corresponding ones of $B \to PV$ decays. It can be understood from Eq. (4) that in addition to the factorizable amplitude of QCD-penguin emission topology, there is a large chiral enhanced penguin contribution in $B \to PP$ modes; while there is no such contribution in $B \to PV$ modes and a negative contribution in $B \to VP$ modes.

Similar to the conventional topological diagram approach [17], the long-standing puzzle of the large $B^0 \to \pi^0\pi^0$ branching fraction can be resolved well attributed to the appropriate magnitude and phase of C in FAT. The QCDF [27] gives the magnitude of $C = \alpha_2 = 0.20^{+0.17}_{-0.11}$ by perturbative calculation, which is only half the size of FAT extracted from experimental data. This may due to the large power corrections or large non-perturbative contribution such as final state interaction and re-scattering effects. With a larger $B^0 \to \pi^0\pi^0$ branching fraction, the $B^0 \to \pi^0\rho^0$ and $B^0 \to \rho^0\rho^0$ branching ratio will grow easily much larger than the experimental data. Actually, only the Glauber phase factor [13], associated with the Goldstone boson π, can resolve the $B \to \pi\pi$, $B \to \pi\rho$, and $B \to \rho\rho$ puzzles consistently. We reproduce these branching ratios correctly

Table 4 Branching fractions ($\times 10^{-6}$) of various $\bar{B} \to PP$ decay modes. We also show the experimental data [26] and results from conventional flavor diagram approach [17] for comparison

Mode	Amplitudes	Exp	This work	Flavor diagram
$\pi^-\pi^0$	T, C, P_{EW}	$5.5 \pm 0.4^\star$	$5.08 \pm 0.39 \pm 1.02 \pm 0.02$	5.40 ± 0.79
$\pi^-\eta$	T, C, P, P_C, P_{EW}	$4.02 \pm 0.27^\star$	$4.13 \pm 0.25 \pm 0.64 \pm 0.01$	3.88 ± 0.39
$\pi^-\eta'$	T, C, P, P_C, P_{EW}	$2.7 \pm 0.9^\star$	$3.37 \pm 0.21 \pm 0.49 \pm 0.01$	5.59 ± 0.54
$\pi^+\pi^-$	$T, E, (P_E), P$	$5.12 \pm 0.19^\star$	$5.15 \pm 0.36 \pm 1.31 \pm 0.14$	5.17 ± 1.03
$\pi^0\pi^0$	$C, E, P, (P_E), P_{EW}$	$1.91 \pm 0.22^\star$	$1.94 \pm 0.30 \pm 0.28 \pm 0.05$	1.88 ± 0.42
$\pi^0\eta$	$C, E, P_C, (P_E), P_{EW}$	$4.3 + 1.8 - 1.7$	$0.86 \pm 0.08 \pm 0.08 \pm 0.04$	0.56 ± 0.03
$\pi^0\eta'$	$C, E, P_C, (P_E), P_{EW}$	1.2 ± 0.6	$0.87 \pm 0.08 \pm 0.10 \pm 0.03$	1.21 ± 0.16
$\eta\eta$	$C, E, P_C, (P_E), P_{EW}$	<1.0	$0.44 \pm 0.09 \pm 0.08 \pm 0.005$	0.77 ± 0.12
$\eta\eta'$	$C, E, P_C, (P_E), P_{EW}$	<1.2	$0.77 \pm 0.13 \pm 0.14 \pm 0.008$	1.99 ± 0.26
$\eta'\eta'$	$C, E, P_C, (P_E), P_{EW}$	<1.7	$0.38 \pm 0.05 \pm 0.07 \pm 0.003$	1.60 ± 0.20
K^-K^0	P	$1.31 \pm 0.17^\star$	$1.32 \pm 0.04 \pm 0.26 \pm 0.01$	1.03 ± 0.02
$K^0\bar{K}^0$	P	$1.21 \pm 0.16^\star$	$1.23 \pm 0.03 \pm 0.25 \pm 0.01$	0.89 ± 0.11
$\pi^-\bar{K}^0$	P	$23.7 \pm 0.8^\star$	$23.2 \pm 0.6 \pm 4.6 \pm 0.2$	23.53 ± 0.42
π^0K^-	T, C, P, P_{EW}	$12.9 \pm 0.5^\star$	$12.8 \pm 0.32 \pm 2.35 \pm 0.10$	12.71 ± 1.05
ηK^-	T, C, P, P_C, P_{EW}	$2.4 \pm 0.4^\star$	$2.0 \pm 0.13 \pm 1.19 \pm 0.03$	1.93 ± 0.31
$\eta' K^-$	T, C, P, P_C, P_{EW}	$70.6 \pm 2.5^\star$	$70.1 \pm 4.7 \pm 11.3 \pm 0.22$	70.92 ± 8.54
π^+K^-	T, P	$19.6 \pm 0.5^\star$	$19.8 \pm 0.54 \pm 4.0 \pm 0.2$	20.2 ± 0.39
$\pi^0\bar{K}^0$	C, P, P_{EW}	$9.9 \pm 0.5^\star$	$8.96 \pm 0.26 \pm 1.96 \pm 0.09$	9.73 ± 0.82
$\eta\bar{K}^0$	C, P, P_C, P_{EW}	$1.23 \pm 0.27^\star$	$1.35 \pm 0.10 \pm 1.02 \pm 0.03$	1.49 ± 0.27
$\eta'\bar{K}^0$	C, P, P_C, P_{EW}	$66 \pm 4^\star$	$66.4 \pm 4.5 \pm 10.6 \pm 0.21$	66.51 ± 7.97

in Table 4 with not too large χ^C. $|T^{\pi\pi}| : |C^{\pi\pi}| = 1 : 0.47$ shown in Eq. (20) is not as large as [17], where the ratio even reached 0.97 in Scheme C.

The $B^- \to K^-K^0$, $B^0 \to K^0\bar{K}^0$ decays are purely penguin decays. From Table 4 one can see that their branching fractions given in the FAT approach are in much better agreement with experimental data than the previous conventional flavor diagram approach [17]. The penguin amplitude is mostly determined by the more precise measurements of $B^0 \to \pi K$ decays. There is only a $SU(3)$ breaking effect between the KK final states and the πK final states. Our results for the KK final sates are larger, because we considered the $SU(3)$ breaking effect and the previous conventional flavor diagram approach did not. For the $B \to PV$ decays, where a vector meson is emitted from the weak interaction point, such as $B^- \to K^-K^{*0}$, $\bar{B}^0 \to K^{*0}\bar{K}^0$ decay modes, there is an extra penguin annihilation diagram P_A, in addition to the penguin emission diagram P. We find that the theoretical prediction for $\mathrm{B}(B^- \to K^-K^{*0})$ is a little larger than $\mathrm{B}(B^- \to K^{*-}K^0)$, and $\mathrm{B}(\bar{B}^0 \to \bar{K}^0K^{*0})$ is a little larger than $\mathrm{B}(\bar{B}^0 \to \bar{K}^{*0}K^0)$. All these results are larger than the previous conventional flavor diagram approach [17], but in agreement with the prediction from SCET [25].

We did not show the decay $\bar{B}^0 \to K^+K^-$ in our table. This decay is measured with $\mathrm{B}(\bar{B}^0 \to K^+K^-) = 0.13 \pm 0.05$, which is less than 3σ significance, therefore, we did not include this measurement into our χ^2 fit program. Theoretically, this decay is dominated by the exchange diagram E and penguin-exchange diagram P_E. Since there is not enough experimental data to fit the P_E contribution, our result for this channel is only from the W-exchange diagram χ^E fitted from the $B^0 \to \pi^0\pi^0(\rho^0)$, $\pi^+\pi^-$ decay modes. With only one contribution, our result $\mathrm{B}(B^0 \to K^+K^-) = 1.30 \pm 0.25 \pm 0.00 \pm 0.13$ is one order of magnitude higher than the central value of experimental data. This should be resolved with more precise experimental data to fit the P_E contribution in the future.

The $B \to PP$ decays with flavor singlet mesons $\eta^{(\prime)}$ in the final states are more complicated than other decay channels. There are complicated η–η' mixing effects and most of them include almost all kinds of topologies except for the E diagram. As shown in Eq. (29), $|P_C|/|P|$ is close to $|C|/|T|$ in ηK decays. The flavor-singlet QCD-penguin diagram P_C in the FAT approach and also in the conventional topological diagram approach [17] plays the same role as the long-distance charm penguin A^{PP}_{ccg}, A^{VP}_{ccg} in SCET [25]. It has an important effect on the large branching fraction of $B \to K\eta'$ and other observations of this type of penguin-dominant decays. In the conventional topological diagram approach, the η–η' mixing angle ϕ is a free parameter to be

Table 5 Branching fractions ($\times 10^{-6}$) of various $\bar{B} \to PV$ decay modes. We also show the experimental data [26] and results from conventional flavor diagram approach [17] for comparison

Mode	Amplitudes	Exp	This work	Flavor diagram
$\pi^-\rho^0$	T, C', P, P_A, P_{EW}	$8.3 \pm 1.2^\star$	$8.6 \pm 1.81 \pm 1.38 \pm 0.03$	7.59 ± 1.41
$\pi^-\omega$	$T, C', P, P'_C, P_A, P_{EW}$	$6.9 \pm 0.5^\star$	$6.78 \pm 1.46 \pm 1.09 \pm 0.02$	7.03 ± 1.42
$\pi^-\phi$	P'_C, P_{EW}	<0.15	$0.28 \pm 0.004 \pm 0.055 \pm 0.003$	0.04 ± 0.02
$\pi^0\rho^-$	T, C, P, P_A, P_{EW}	$10.9 \pm 1.4^\star$	$12.9 \pm 0.73 \pm 2.30 \pm 0.12$	12.15 ± 2.52
$\eta\rho^-$	$T, C, P, P_C, P_A, P_{EW}$	7.0 ± 2.9	$8.16 \pm 0.48 \pm 1.43 \pm 0.07$	5.26 ± 1.19
$\eta'\rho^-$	$T, C, P, P_C, P_A, P_{EW}$	$9.7 \pm 2.2^\star$	$6.0 \pm 0.34 \pm 0.97 \pm 0.05$	5.66 ± 1.25
$\pi^+\rho^-$	$T, E, P, (P_E), P_A$	$14.6 \pm 1.6^\star$	$12.4 \pm 0.64 \pm 3.20 \pm 0.38$	15.20 ± 1.52
$\pi^-\rho^+$	$T, E, P, (P_E)$	$8.4 \pm 1.1^\star$	$6.04 \pm 0.47 \pm 1.70 \pm 0.25$	8.22 ± 1.06
$\pi^0\rho^0$	$C, C', E, P, P_A, (P_E), P_{EW}$	$2 \pm 0.5^\star$	$1.32 \pm 0.47 \pm 0.09 \pm 0.14$	2.24 ± 0.93
$\pi^0\omega$	$C, C', E, P, P_A, (P_E), P_{EW}$	<0.5	$2.31 \pm 0.88 \pm 0.24 \pm 0.07$	1.02 ± 0.66
$\pi^0\phi$	P'_C, P_{EW}	<0.15	$0.13 \pm 0.002 \pm 0.025 \pm 0.001$	0.02 ± 0.01
$\eta\rho^0$	$C, C', E, P, P_C, P'_C, P_A, (P_E), P_{EW}$	<1.5	$4.41 \pm 1.15 \pm 0.39 \pm 0.17$	0.54 ± 0.32
$\eta\omega$	$C, C', E, P, P_C, P'_C, P_A, (P_E), P_{EW}$	$0.94^{+0.40}_{-0.31}$	$0.89 \pm 0.30 \pm 0.08 \pm 0.09$	1.12 ± 0.44
$\eta\phi$	P'_C, P_{EW}	<0.5	$0.077 \pm 0.001 \pm 0.015 \pm 0.0008$	0.01 ± 0.01
$\eta'\rho^0$	$C, C', E, P, P_C, P'_C, (P_E), P_{EW}$	<1.3	$3.19 \pm 0.77 \pm 0.29 \pm 0.12$	0.63 ± 0.33
$\eta'\omega$	$C, C', E, P, P_C, P'_C, (P_E), P_{EW}$	$1.0^{+0.5}_{-0.4}$	$0.95 \pm 0.21 \pm 0.05 \pm 0.06$	1.24 ± 0.47
$\eta'\phi$	P'_C, P_{EW}	<0.5	$0.05 \pm 0.0008 \pm 0.01 \pm 0.0005$	0.01 ± 0.01
K^-K^{*0}	P, P_A	<1.1	$0.59 \pm 0.06 \pm 0.10 \pm 0.01$	0.46 ± 0.03
K^0K^{*-}	P		$0.44 \pm 0.03 \pm 0.09 \pm 0.004$	0.31 ± 0.03
$K^0\bar{K}^{*0}$	P		$0.41 \pm 0.02 \pm 0.08 \pm 0.004$	0.29 ± 0.03
$\bar{K}^0K^{*0}$	P, P_A		$0.55 \pm 0.05 \pm 0.09 \pm 0.01$	0.43 ± 0.02
$\pi^-\bar{K}^{*0}$	P, P_A	$10.1 \pm 0.9^\star$	$10.0 \pm 0.95 \pm 1.78 \pm 0.15$	10.47 ± 0.60
π^0K^{*-}	T, C, P, P_A, P_{EW}	$8.2 \pm 1.9^\star$	$6.23 \pm 0.51 \pm 0.98 \pm 0.07$	9.79 ± 2.95
ηK^{*-}	$T, C, P, P_C, P_A, P_{EW}$	$19.3 \pm 1.6^\star$	$17.3 \pm 0.8 \pm 2.4 \pm 0.3$	16.57 ± 2.58
$\eta' K^{*-}$	$T, C, P, P_C, P_A, P_{EW}$	$4.8^{+1.8}_{-1.6}$	$3.31 \pm 0.44 \pm 0.38 \pm 0.13$	3.43 ± 1.43
$K^-\rho^0$	T, C', P, P_{EW}	$3.7 \pm 0.5^\star$	$3.97 \pm 0.25 \pm 0.80 \pm 0.04$	3.97 ± 0.90
$K^-\omega$	T, C', P, P'_C, P_{EW}	$6.5 \pm 0.4^\star$	$6.52 \pm 0.73 \pm 1.13 \pm 0.06$	6.43 ± 1.49
$K^-\phi$	P, P'_C, P_A, P_{EW}	$8.8 \pm 0.7^\star$	$8.38 \pm 1.21 \pm 0.69 \pm 0.50$	8.34 ± 1.31
$\bar{K}^0\rho^-$	P	$8 \pm 1.5^\star$	$7.74 \pm 0.47 \pm 1.55 \pm 0.07$	7.09 ± 0.77
π^+K^{*-}	T, P, P_A	$8.4 \pm 0.8^\star$	$8.40 \pm 0.77 \pm 1.46 \pm 0.14$	8.35 ± 0.50
$\pi^0\bar{K}^{*0}$	C, P, P_A, P_{EW}	$3.3 \pm 0.6^\star$	$3.35 \pm 0.36 \pm 0.65 \pm 0.08$	3.89 ± 1.98
$\eta\bar{K}^{*0}$	C, P, P_C, P_A, P_{EW}	$15.9 \pm 1^\star$	$16.6 \pm 0.7 \pm 2.3 \pm 0.3$	16.34 ± 2.48
$\eta'\bar{K}^{*0}$	$C, P, P_C, P'_C, P_A, P_{EW}$	$2.8 \pm 0.6^\star$	$3.0 \pm 0.5 \pm 0.3 \pm 0.1$	3.14 ± 1.24
$K^-\rho^+$	T, P	$7 \pm 0.9^\star$	$8.27 \pm 0.44 \pm 1.65 \pm 0.07$	8.28 ± 0.80
$\bar{K}^0\rho^0$	C', P, P_{EW}	$4.7 \pm 0.4^\star$	$4.59 \pm 0.34 \pm 0.79 \pm 0.04$	4.97 ± 1.14
$\bar{K}^0\omega$	C', P, P'_C, P_{EW}	$4.8 \pm 0.6^\star$	$4.80 \pm 0.61 \pm 0.95 \pm 0.05$	4.82 ± 1.26
$\bar{K}^0\phi$	P, P'_C, P_A, P_{EW}	$7.3 \pm 0.7^\star$	$7.77 \pm 1.12 \pm 0.64 \pm 0.46$	7.72 ± 1.21

fitted from hadronic B decay data as $\phi = 46^\circ$ for $B \to PP$ and $\phi = 43^\circ$ for $B \to PV$ decays [17]. However, the fitting is not so successful as expected with the branching faction of $B^- \to \pi^-\eta'$ twice larger than the experimental value. These decays were recently reanalyzed with better results for $B \to PP$ decays in Ref. [14]. It is noted that we fix the mixing angles from other experiments for the η–η' case, leading to better results for these decays.

For the sub-leading contribution electroweak penguin diagram P_{EW}, four free parameters (two magnitudes and two phases) are introduced to be fitted from experiments [17] with non-negligible strong phase for $B \to PP$ decays and

even considerable magnitude for $B \to VP$ decays. As stated in the last section, we did not include any free parameters for this kind of diagrams but use factorization formulas to make predictions. For the $B \to \pi(\rho)K(K^*)$ decays, their branching fractions are in good agreement with data by the non-negligible factorization P_{EW} diagram contribution. For example, the central value of $\mathrm{B}(B^- \to \pi^0 K^-)$ is equal to data precisely attributed to the non-negligible correction effect from the P_{EW} diagram.

Most of the $B_s \to PP, PV$ decays are not well measured in the experiments. Therefore, we do not include any of the B_s data in our χ^2 fit program. Their branching ratios are all as predictions in our FAT approach shown in Table 6. The accuracy of these predictions relies on the assumption that the mechanisms for the B and B_s decays are the same. If there are enough data for B_s decays, one needs to do the χ^2 fit again. In this table, we do not include the channel $B_s \to \pi^+\pi^-$. Our result (with only W-exchange contribution) for this channel $\mathrm{B}(\bar{B}_s \to \pi^+\pi^-) = 0.051 \pm 0.001 \pm 0 \pm 0.005$ is much smaller than the experimental data measured by LHCb and CDF shown in Eq. (6). As stated in the last section, this decay is dominated by the penguin-exchange diagram P_E [88–90], which can only be fitted from this mode $B_s \to \pi^+\pi^-$. One measurement to determine one parameter is not a perfect way of χ^2 fitting. Therefore we look forward to more data to determine this contribution in other modes and to test our

Table 6 Branching fractions ($\times 10^{-6}$) of various $\bar{B}_s \to PP$ and $\bar{B}_s \to PV$ decays. We also show the experimental data [26] and results from conventional flavor diagram approach [17] for comparison

Mode	Amplitudes	Exp	This work	Flavor diagram
$\pi^- K^+$	T, P	5.5 ± 0.6	$6.98 \pm 0.02 \pm 1.40 \pm 0.02$	5.86 ± 0.78
$\pi^0\eta$	$C, E, P_C, (P_E), P_{EW}$	<1000	$0.10 \pm 0.013 \pm 0.013 \pm 0.003$	0.12 ± 0.07
$\pi^0\eta'$	$C, E, P_C, (P_E), P_{EW}$		$0.11 \pm 0.01 \pm 0.02 \pm 0.002$	0.12 ± 0.06
$\pi^0 K^0$	C, P, P_{EW}		$0.97 \pm 0.16 \pm 0.2 \pm 0.003$	2.25 ± 0.33
$\eta\eta$	$C, E, P, P_C, (P_E), P_{EW}$	<1500	$11.4 \pm 0.42 \pm 2.25 \pm 0.04$	8.24 ± 1.53
$\eta\eta'$	$C, E, P, P_C, (P_E), P_{EW}$		$40.4 \pm 2.06 \pm 8.14 \pm 0.13$	33.47 ± 3.64
ηK^0	C, P, P_C, P_{EW}		$0.55 \pm 0.11 \pm 0.08 \pm 0.002$	0.97 ± 0.16
$\eta'\eta'$	$C, E, P, P_C, (P_E), P_{EW}$		$42.1 \pm 3.48 \pm 8.38 \pm 0.13$	41.48 ± 6.25
$\eta' K^0$	C, P, P_C, P_{EW}		$2.15 \pm 0.15 \pm 0.30 \pm 0.01$	3.94 ± 0.39
K^+K^-	$T, E, P, (P_E)$	24.9 ± 1.7	$16.7 \pm 0.46 \pm 3.27 \pm 0.16$	17.90 ± 2.98
$K^0\bar{K}^0$	P	<66	$17.5 \pm 0.47 \pm 3.50 \pm 0.16$	17.48 ± 2.36
$\pi^- K^{*+}$	T, P		$11.1 \pm 0.02 \pm 2.21 \pm 0.03$	7.92 ± 1.02
$\pi^0\phi$	C, P_{EW}		$0.26 \pm 0.02 \pm 0.05 \pm 0.001$	1.94 ± 1.14
$\pi^0 K^{*0}$	C, P, P_{EW}		$1.22 \pm 0.25 \pm 0.24 \pm 0$	3.07 ± 1.20
$\eta\rho^0$	$C', E, P'_C, (P_E), P_{EW}$		$0.13 \pm 0.02 \pm 0.02 \pm 0.003$	0.34 ± 0.21
$\eta\omega$	$C', E, P'_C, (P_E), P_{EW}$		$3.25 \pm 0.10 \pm 0.63 \pm 0.03$	0.15 ± 0.16
$\eta\phi$	$C, P, P_C, P'_C, P_{EW}, P_A$		$0.80 \pm 0.22 \pm 0.53 \pm 0.14$	0.39 ± 0.39
ηK^{*0}	C, P, P_C, P_{EW}, P_A		$0.99 \pm 0.18 \pm 0.16 \pm 0.01$	1.44 ± 0.54
$\eta'\rho^0$	$C', E, P'_C, (P_E), P_{EW}$		$0.37 \pm 0.07 \pm 0.05 \pm 0.01$	0.31 ± 0.19
$\eta'\omega$	$C', E, P'_C, (P_E), P_{EW}$		$3.97 \pm 0.15 \pm 0.79 \pm 0.04$	0.14 ± 0.14
$\eta'\phi$	$C, P, P_C, P'_C, P_{EW}, P_A$		$13.0 \pm 1.05 \pm 0.98 \pm 0.67$	5.48 ± 1.84
$\eta' K^{*0}$	C, P, P_C, P_{EW}, P_A		$1.64 \pm 0.15 \pm 0.22 \pm 0.03$	1.65 ± 0.60
$K^+\rho^-$	T, P, P_A		$17.5 \pm 0 \pm 3.5 \pm 0.2$	14.63 ± 1.46
K^+K^{*-}	$T, E, P, P_A, (P_E)$		$8.85 \pm 1.06 \pm 1.04 \pm 0.37$	8.03 ± 0.48
K^-K^{*+}	$T, E, P, (P_E)$		$6.39 \pm 0.38 \pm 1.35 \pm 0.07$	7.98 ± 0.77
$K^0\rho^0$	C', P, P'_C, P_A, P_{EW}		$1.61 \pm 1.10 \pm 0.31 \pm 0.02$	0.56 ± 0.24
$K^0\omega$	C', P, P'_C, P_A, P_{EW}		$1.43 \pm 0.88 \pm 0.25 \pm 0.02$	0.58 ± 0.25
$K^0\phi$	P, P'_C, P_{EW}		$0.35 \pm 0.04 \pm 0.06 \pm 0.003$	0.41 ± 0.07
$K^0\bar{K}^{*0}$	P, P_A		$9.28 \pm 1.14 \pm 1.21 \pm 0.34$	9.33 ± 0.54
$\bar{K}^0 K^{*0}$	P		$6.31 \pm 0.38 \pm 1.26 \pm 0.06$	6.32 ± 0.68

Table 7 The direct *CP* asymmetries ($\mathcal{A}$) and mixing-induced *CP* asymmetries ($\mathcal{S}$) of $\bar{B} \to PP$ decays. We also show the results from conventional flavor diagram approach [17] for comparison

Mode	$\mathcal{A}_{\rm exp}$	$\mathcal{A}_{\rm this\ work}$	$\mathcal{A}_{\rm Flavor\ diagram}$	$\mathcal{S}_{\rm exp}$	$\mathcal{S}_{\rm this\ work}$	$\mathcal{S}_{\rm Flavor\ diagram}$
$\pi^+\pi^-$	$0.31 \pm 0.05^\star$	0.31 ± 0.04	0.326 ± 0.081	$-0.67 \pm 0.06^\star$	-0.60 ± 0.03	-0.717 ± 0.061
$\pi^0\pi^0$	0.43 ± 0.24	0.57 ± 0.06	0.611 ± 0.113		0.58 ± 0.06	0.454 ± 0.112
$\pi^0\eta$		-0.16 ± 0.16	0.566 ± 0.114		-0.98 ± 0.04	-0.098 ± 0.338
$\pi^0\eta'$		0.39 ± 0.14	0.385 ± 0.114		-0.90 ± 0.07	0.142 ± 0.234
$\eta\eta$		-0.85 ± 0.06	-0.405 ± 0.129		0.33 ± 0.12	-0.796 ± 0.077
$\eta\eta'$		-0.97 ± 0.04	-0.394 ± 0.117		-0.20 ± 0.15	-0.903 ± 0.049
$\eta'\eta'$		-0.87 ± 0.07	-0.122 ± 0.136		-0.46 ± 0.14	-0.964 ± 0.037
$\pi^0 K_s$	0.00 ± 0.13	-0.14 ± 0.03	-0.173 ± 0.019	$0.58 \pm 0.17^\star$	0.73 ± 0.01	0.754 ± 0.014
ηK_s		-0.30 ± 0.10	-0.301 ± 0.041		0.68 ± 0.04	0.592 ± 0.035
$\eta' K_s$	0.06 ± 0.04	0.030 ± 0.004	0.022 ± 0.006	$0.63 \pm 0.06^\star$	0.69 ± 0.00	0.685 ± 0.004
$K^0\bar{K}^0$		-0.057 ± 0.002	0.017 ± 0.041	0.8 ± 0.5	0.099 ± 0.002	0
$\pi^-\pi^0$	0.03 ± 0.04	-0.026 ± 0.003	0.069 ± 0.027			
$\pi^-\eta$	-0.14 ± 0.07	-0.14 ± 0.07	-0.081 ± 0.074			
$\pi^-\eta'$	0.06 ± 0.16	0.37 ± 0.07	0.374 ± 0.087			
$\pi^-\bar{K}^0$	-0.017 ± 0.016	0.0027 ± 0.0001	0			
$\pi^0 K^-$	0.037 ± 0.021	0.065 ± 0.024	0.047 ± 0.025			
ηK^-	$-0.37 \pm 0.08^\star$	-0.22 ± 0.08	-0.426 ± 0.043			
$\eta' K^-$	0.013 ± 0.017	-0.021 ± 0.007	-0.027 ± 0.008			
K^-K^0	-0.21 ± 0.14	-0.057 ± 0.002	0			
π^+K^-	$-0.082 \pm 0.006^\star$	-0.081 ± 0.005	-0.080 ± 0.011			

FAT in the future. Similarly, without this contribution, we are unable to predict a number of decay channels, dominated by this contribution: $B^0 \to K^+K^-$, $B^0 \to K^{*+}K^-$, $B^0 \to K^+K^{*-}$, $B_s \to \pi^+\rho^-$, $B_s \to \pi^-\rho^+$, $B_s \to \pi^0\rho^0$, $B_s \to \pi^0\omega$, and $B_s \to \pi^0\pi^0$.

3.4 *CP* asymmetry study

The charmless B decays are important mostly because of the large direct *CP* asymmetry in B decays. Due to the CKM matrix elements suppression of the tree diagram, the penguin diagram contribution is at the same order of magnitude as the tree diagram. The large CKM phase difference between these two kinds of diagram almost guarantees the existence of a large direct *CP* asymmetry. That is not the whole story. The direct *CP* asymmetry parameter is also proportional to the strong phase difference between these two diagrams. Unfortunately, the strong phase is mostly from non-perturbative QCD dynamics. That is the reason why QCD factorization approaches and SCET can predict the branching ratios of the charmless B decays well but make wrong predictions or no prediction for the direct *CP* asymmetries. There are already three good measurements of direct *CP* asymmetry measurements in $B \to PP$ decays and three in $B \to PV$ decays indicated by a star in Tables 7 and 8. There are also five mixing-induced *CP* asymmetry measurements for the neutral B meson decays to be used in our χ^2 program. We give the direct *CP* and mixing-induced *CP* asymmetries of corresponding B decay modes in Tables 7 and 8. From the *CP* asymmetry formula in Eq. (11), we know that the *CP* asymmetry is proportional to the difference of B meson and $\bar{B}$ meson. Thus the theoretical uncertainty from hadronic parameters mostly cancel, because they contribute to the charge conjugate modes equally. The main theoretical uncertainty for the *CP* asymmetry parameters is from the experimental data and CKM angle. We did not show the individual uncertainty, but we show the combined one in these *CP* asymmetry tables.

Since the CKM matrix elements are enhanced for the penguin diagram compared with the tree diagrams in the $B \to \pi(\rho)K^{(*)}$ decays by $b \to s$ transition, there is large interference effect between these two kinds of Feynman diagrams, which results in larger *CP* asymmetry in these decays. $A_{CP}(\bar{B}^0 \to \pi^+K^-)$ is the first measurement of direct *CP* asymmetry in B decays. From Table 4, one can see that the $B^- \to \pi^0K^-$ decay has the same dominant decay amplitude T and P as the $\bar{B}^0 \to \pi^+K^-$ decay, thus one expects the same direct *CP* asymmetry [10]. However, experimentally these two direct *CP* asymmetries are quite different, even having an opposite sign. This is the so-called πK *CP*-puzzle.

Table 8 The direct *CP* asymmetries ($\mathcal{A}$) and mixing-induced *CP* asymmetries ($\mathcal{S}$) of $\bar{B} \to PV$ decays. We also show the results from conventional flavor diagram approach [17] for comparison

Mode	$\mathcal{A}_{\rm exp}$	$\mathcal{A}_{\rm this\ work}$	$\mathcal{A}_{\rm Flavor\ diagram}$	$\mathcal{S}_{\rm exp}$	$\mathcal{S}_{\rm this\ work}$	$\mathcal{S}_{\rm Flavor\ diagram}$
$\pi^+\rho^-$	0.13 ± 0.06	0.15 ± 0.03	0.120 ± 0.027	0.07 ± 0.14	0.011 ± 0.034	-0.049 ± 0.074
$\pi^-\rho^+$	-0.08 ± 0.08	-0.44 ± 0.03	-0.136 ± 0.053	0.05 ± 0.08	-0.093 ± 0.040	-0.024 ± 0.065
$\pi^0\rho^0$	-0.27 ± 0.24	0.36 ± 0.08	-0.043 ± 0.121	-0.23 ± 0.34	0.19 ± 0.16	-0.229 ± 0.112
$\pi^0\omega$		-0.024 ± 0.068	-0.188 ± 0.185		0.29 ± 0.05	-0.315 ± 0.195
$\eta\rho^0$		-0.23 ± 0.03	-0.264 ± 0.215		-0.023 ± 0.038	-0.628 ± 0.196
$\eta\omega$		-0.30 ± 0.13	0.054 ± 0.137		0.43 ± 0.09	-0.461 ± 0.113
$\eta'\rho^0$		0.088 ± 0.085	-0.440 ± 0.317		-0.48 ± 0.07	-0.714 ± 0.252
$\eta'\omega$		-0.85 ± 0.17	-0.005 ± 0.259		0.50 ± 0.26	-0.624 ± 0.120
$K_s\rho^0$	0.04 ± 0.20	-0.085 ± 0.059	0.069 ± 0.053	0.5 ± 0.21	0.88 ± 0.05	0.643 ± 0.036
$K_s\omega$	0 ± 0.4	0.25 ± 0.10	-0.053 ± 0.055	$0.7 \pm 0.21^\star$	0.70 ± 0.04	0.789 ± 0.028
$K_s\phi$	-0.01 ± 0.14	-0.006 ± 0.001	0	$0.59 \pm 0.14^\star$	0.70 ± 0.00	0.718 ± 0.000
$\bar{K}^0K^{*0}$		-0.10 ± 0.02	0		-0.90 ± 0.03	0
$K^0\bar{K}^{*0}$		-0.18 ± 0.01	0		0.89 ± 0.03	0
$\pi^-\rho^0$	$0.18^{+0.09}_{-0.17}$	-0.45 ± 0.04	-0.239 ± 0.084			
$\pi^-\omega$	-0.04 ± 0.06	0.054 ± 0.052	0.075 ± 0.067			
$\pi^0\rho^-$	0.02 ± 0.11	0.16 ± 0.02	0.053 ± 0.094			
$\eta\rho^-$	0.11 ± 0.11	-0.11 ± 0.02	0.162 ± 0.072			
$\eta'\rho^-$	0.26 ± 0.17	0.45 ± 0.05	0.223 ± 0.137			
$\pi^-\bar{K}^{*0}$	-0.04 ± 0.09	0.005 ± 0.001	0			
π^0K^{*-}	-0.06 ± 0.24	0.088 ± 0.040	-0.116 ± 0.092			
ηK^{*-}	0.02 ± 0.06	-0.17 ± 0.02	-0.016 ± 0.037			
$\eta' K^{*-}$	-0.26 ± 0.27	-0.45 ± 0.09	-0.391 ± 0.162			
$K^-\rho^0$	$0.37 \pm 0.10^\star$	0.59 ± 0.06	0.306 ± 0.100			
$K^-\omega$	0.02 ± 0.05	0.19 ± 0.09	0.010 ± 0.080			
$K^-\phi$	0.04 ± 0.04	-0.006 ± 0.001	0			
K^-K^{*0}		-0.10 ± 0.02	0			
K^0K^{*-}		-0.18 ± 0.01	0			
$\bar{K}^0\rho^-$	-0.12 ± 0.17	0.009 ± 0.000	0			
π^+K^{*-}	$-0.22 \pm 0.06^\star$	-0.20 ± 0.04	-0.217 ± 0.048			
$\pi^0\bar{K}^{*0}$	-0.15 ± 0.13	-0.27 ± 0.05	-0.332 ± 0.114			
$\eta\bar{K}^{*0}$	$0.19 \pm 0.05^\star$	0.065 ± 0.011	0.099 ± 0.028			
$\eta'\bar{K}^{*0}$	-0.07 ± 0.18	0.059 ± 0.049	0.069 ± 0.152			
$K^-\rho^+$	0.21 ± 0.11	0.59 ± 0.01	0.134 ± 0.053			

In our study, the sub-leading contribution C is twice bigger than that in the QCDF, especially with a large strong phase. This again implies large power corrections or large non-perturbative QCD corrections in the C diagram of $B \to \pi K$ decays.

There is one category of decays with pure penguin contributions, such as $B^- \to K^-K^0$, $\bar{B}^0 \to K^0\bar{K}^0$, $B^- \to \pi^-\bar{K}^0$, $B^- \to \pi^-\bar{K}^{*0}$, $B^- \to \rho^-\bar{K}^0$ and $\bar{B}_s \to K^0\bar{K}^0$. Their direct *CP* asymmetry is expected to be zero, at leading-order approximation. The very small (not zero) *CP* asymmetry is from the small up quark or charm quark penguin contribution interference with the dominant top quark contribution. Any large *CP* asymmetry measurement for these decays will be a clear signal of new physics. In Table 7, we did not show the decay channel $\bar{B}^0 \to K^+K^-$. The reason is that there should be two major contributions for this channel, but we calculate only one (tree level W exchange diagram). The other contribution from penguin-exchange (P_E) diagram is not fitted because of lack of experimental data. The branching ratio of this channel with only one contribution, discussed in previous subsection, is far from the central value of experimental data. This may indicate the importance

Table 9 The direct *CP* asymmetries ($\mathcal{A}$) and mixing-induced *CP* asymmetries ($\mathcal{S}$) of $\bar{B}_s \to PP$ decays. We also show the results from conventional flavor diagram approach [17] for comparison

Mode	$\mathcal{A}_{\rm exp}$	$\mathcal{A}_{\rm this\ work}$	$\mathcal{A}_{\rm Flavor\ diagram}$	$\mathcal{S}_{\rm exp}$	$\mathcal{S}_{\rm this\ work}$	$\mathcal{S}_{\rm Flavor\ diagram}$
$\pi^0\eta$		0.90 ± 0.05	-0.165 ± 0.292		0.19 ± 0.11	0.836 ± 0.198
$\pi^0\eta'$		0.44 ± 0.10	0.259 ± 0.335		-0.79 ± 0.07	0.953 ± 0.116
$\pi^0 K_s$		0.87 ± 0.05	0.724 ± 0.054		0.0096 ± 0.0905	0.302 ± 0.080
$\eta\eta$		-0.11 ± 0.01	-0.116 ± 0.018		-0.14 ± 0.01	-0.095 ± 0.020
$\eta\eta'$		-0.013 ± 0.005	-0.009 ± 0.003		-0.038 ± 0.006	-0.036 ± 0.007
ηK_s		0.74 ± 0.17	0.452 ± 0.057		0.31 ± 0.16	0.787 ± 0.042
$\eta'\eta'$		0.042 ± 0.006	0.016 ± 0.009		-0.055 ± 0.006	0.028 ± 0.009
$\eta' K_s$		-0.58 ± 0.06	-0.367 ± 0.089		-0.029 ± 0.099	0.191 ± 0.090
K^+K^-	-0.14 ± 0.11	-0.11 ± 0.02	-0.090 ± 0.021	0.30 ± 0.13	0.097 ± 0.022	0.140 ± 0.030
$K^0\bar{K}^0$		0.0027 ± 0.0001	-0.075 ± 0.035		0.069 ± 0.000	-0.039 ± 0.001
π^-K^+	0.28 ± 0.04	0.16 ± 0.01	0.266 ± 0.033			

of the penguin-exchange (P_E) diagram, which will give a large direct *CP* asymmetry for this channel. Similarly, we cannot predict the *CP* asymmetry for $B^0 \to K^{*+}K^-$ and $B^0 \to K^+K^{*-}$.

The mixing-induced *CP*asymmetries in neutral B decays into final *CP* eigenstates are dominated by the B^0–$\bar{B}^0$ mixing phase with little dependence on strong phases. That is the reason why it is usually used for searching possible new physics. For example, the measured mixing-induced *CP* asymmetry parameters of $S_{CP}(\pi^+\pi^-)$, $S_{CP}(\pi^0 K_S)$, $S_{CP}(\eta' K_S)$, and $S_{CP}(\phi K_S)$ have received much attention in experiment and in theoretical aspect due to little theoretical uncertainty. Currently, there is good agreement between theoretical calculations and experimental data shown in Tables 7 and 8. Further study is needed by both theoretical and experimental efforts in the future.

There are only two channels of B_s decays, namely $B_s \to K^+K^-$ and $\bar{B}_s \to K^+\pi^-$ with *CP* asymmetry measurements shown in Table 9. As stated, we do not include any B_s data in our χ^2 fit. All the B_s results are predictions. It is easy to see that our predictions for these two channels agree with the data within error bar. There is no *CP* asymmetry measurement for $B_s \to PV$ decays. Our theoretical predictions are shown in Table 10, together with results from the conventional flavor diagram approach. It is noted that there are large differences between predictions of these two approaches, for example: $B_s \to \pi^0\phi$, $B_s \to \eta\rho^0$, $B_s \to \eta'\rho^0$ and $B_s \to \eta'\omega$ etc. Many of these entries with large *CP* asymmetry predicted can be tested by the experiments in the near future. Similar to the situation of branching ratios, we also did not give predictions for the *CP* asymmetry of decays $B_s \to \pi^+\pi^-$, $B_s \to \pi^+\rho^-$, $B_s \to \pi^-\rho^+$, $B_s \to \pi^0\rho^0$, $B_s \to \pi^0\omega$ and $B_s \to \pi^0\pi^0$, due to lack of information of the penguin-exchange diagram (P_E).

3.5 The flavor SU(3) asymmetry

The flavor $SU(3)$ symmetry is broken by the difference in the u, d, and s quark masses, especially the difference in d and s quark masses. The $SU(3)$ breaking is also very important in explaining the different size of *CP* asymmetry in different charmless $B \to PP$, PV decays. We consider the flavor $SU(3)$ violating contributions assisted by a factorization hypothesis where the source of $SU(3)$ asymmetries are mainly from decay constants and weak transition form factors. It is not necessary to include different $SU(3)$ asymmetry phases for different modes, because our numerical results of branching ratios and *CP* asymmetry parameters are in good agreement with experimental data shown in previous subsections. As every decay mode includes various topological diagrams, the precise flavor $SU(3)$ breaking effects cannot be separated from one another in $B \to PP$, PV decays; they are hard to test by experimental data. We show the flavor $SU(3)$ breaking effect in every topology amplitude between $B \to \pi\pi$ and $B \to \pi K$, $B \to \eta\pi$ and $B \to \eta K$, as follows:

$$\left|\frac{T(B^- \to \pi^0 K^-)}{V_{ub}V_{us}^*}\right| : \left|\frac{T(B^- \to \pi^0\pi^-)}{V_{ub}V_{ud}^*}\right| = 1 : 0.83, \tag{32}$$

$$\left|\frac{C(B^- \to \pi^0 K^-)}{V_{ub}V_{us}^*}\right| : \left|\frac{C(B^- \to \pi^0\pi^-)}{V_{ub}V_{ud}^*}\right| = 1 : 0.91, \tag{33}$$

$$\left|\frac{P(\bar{B}^0 \to \pi^+ K^-)}{V_{tb}V_{ts}^*}\right| : \left|\frac{P(\bar{B}^0 \to \pi^+\pi^-)}{V_{tb}V_{td}^*}\right| = 1 : 0.89, \tag{34}$$

$$\left|\frac{P_C(B^- \to \eta K^-)}{V_{tb}V_{ts}^*}\right| : \left|\frac{P_C(B^- \to \eta\pi^-)}{V_{tb}V_{td}^*}\right| = 1 : 0.91. \tag{35}$$

Table 10 The direct *CP* asymmetries ($\mathcal{A}$) and mixing-induced *CP* asymmetries ($\mathcal{S}$) of $\bar{B}_s \to PV$ decays. We also show the results from conventional flavor diagram approach [17] for comparison

Mode	$\mathcal{A}_{\text{this work}}$	$\mathcal{A}_{\text{Flavor diagram}}$	$\mathcal{S}_{\text{this work}}$	$\mathcal{S}_{\text{Flavor diagram}}$
$\pi^0\phi$	0.89 ± 0.04	0.073 ± 0.201	-0.25 ± 0.07	0.439 ± 0.171
$\eta\rho^0$	-0.46 ± 0.38	0.323 ± 0.136	0.88 ± 0.19	-0.002 ± 0.168
$\eta\omega$	-0.086 ± 0.071	-0.432 ± 0.271	-0.31 ± 0.06	-0.238 ± 0.296
$\eta\phi$	0.083 ± 0.113	0.428 ± 0.504	0.39 ± 0.15	0.534 ± 0.400
$\eta^{'}\rho^0$	-0.67 ± 0.10	0.323 ± 0.136	-0.72 ± 0.07	-0.002 ± 0.168
$\eta^{'}\omega$	0.33 ± 0.06	-0.432 ± 0.271	-0.14 ± 0.07	-0.238 ± 0.296
$\eta^{'}\phi$	-0.010 ± 0.017	0.043 ± 0.090	0.047 ± 0.015	0.166 ± 0.057
K^+K^{*-}	-0.30 ± 0.04	-0.217 ± 0.048	-0.78 ± 0.06	0
K^-K^{*+}	0.39 ± 0.04	0.134 ± 0.053	0.67 ± 0.05	0
$K_s\rho^0$	-0.42 ± 0.15	-0.124 ± 0.453	0.78 ± 0.08	-0.348 ± 0.285
$K_s\omega$	-0.010 ± 0.151	-0.029 ± 0.436	-0.32 ± 0.30	0.928 ± 0.110
$K_s\phi$	-0.003 ± 0.033	0	-0.85 ± 0.01	-0.692 ± 0.000
$K^0\bar{K}^{*0}$	0.002 ± 0.001	0	-0.74 ± 0.05	0
$\bar{K}^0K^{*0}$	0.009 ± 0.000	0	0.83 ± 0.04	0
π^-K^{*+}	-0.30 ± 0.01	-0.136 ± 0.053		
π^0K^{*0}	-0.30 ± 0.06	-0.423 ± 0.158		
ηK^{*0}	0.57 ± 0.12	0.828 ± 0.123		
$\eta^{'}K^{*0}$	-0.46 ± 0.10	-0.408 ± 0.273		
$K^+\rho^-$	0.16 ± 0.03	0.120 ± 0.027		

From the above results, we find that the flavor $SU(3)$ breaking effects are around 10% because of different decay constants between f_π and f_K, or form factors $F^{B\to\pi}$ and $F^{B\to K}$. The flavor $SU(3)$ breaking effect in every topology amplitude between $B \to \pi\rho$ and $B \to \pi K^*$, $B \to \eta\rho$ and $B \to \eta K^*$ are also shown, as follows:

$$\left|\frac{T(B^- \to \pi^0 K^{*-})}{V_{ub}V_{us}^*}\right| : \left|\frac{T(B^- \to \pi^0\rho^-)}{V_{ub}V_{ud}^*}\right| = 1 : 0.83, \tag{36}$$

$$\left|\frac{C(B^- \to K^{*-}\pi^0)}{V_{ub}V_{us}^*}\right| : \left|\frac{C(B^- \to \rho^-\pi^0)}{V_{ub}V_{ud}^*}\right| = 1 : 0.80, \tag{37}$$

$$\left|\frac{P(\bar{B}^0 \to \pi^+ K^{*-})}{V_{tb}V_{ts}^*}\right| : \left|\frac{P(\bar{B}^0 \to \pi^+\rho^-)}{V_{tb}V_{td}^*}\right| = 1 : 0.74, \tag{38}$$

$$\left|\frac{P_C(B^- \to K^{*-}\eta)}{V_{tb}V_{ts}^*}\right| : \left|\frac{P_C(B^- \to \rho^-\eta)}{V_{tb}V_{td}^*}\right| = 1 : 0.80, \tag{39}$$

$$\left|\frac{P_A(\bar{B}^0 \to \pi^+ K^{*-})}{V_{tb}V_{ts}^*}\right| : \left|\frac{P_A(\bar{B}^0 \to \pi^+\rho^-)}{V_{tb}V_{td}^*}\right| = 1 : 0.84. \tag{40}$$

It is easy to see that the flavor $SU(3)$ breaking effects are larger than 20% because of different decay constants between f_ρ and f_{K^*}, or different form factors between $A_0^{B\to\rho}$ and $A_0^{B\to K^*}$.

In previous flavor diagram approach, the charmless $B \to PP$ and $B \to PV$ decays are fitted separately with very different theoretical parameters. That implies a large difference between pseudoscalar meson and vector meson. To show this difference numerically, we have

$$|T(B^- \to \pi^0\pi^-)| : |T(B^- \to \pi^0\rho^-)| = 1 : 1.64, \tag{41}$$

$$|C(B^- \to \pi^0\pi^-)| : |C'(B^- \to \pi^-\rho^0)| = 1 : 1.43, \tag{42}$$

$$|P(\bar{B}^0 \to \pi^+\pi^-)| : |P(\bar{B}^0 \to \pi^+\rho^-)| = 1 : 0.66. \tag{43}$$

It is easy to see that this difference between π and ρ meson emission is indeed much larger than the so-called flavor $SU(3)$ breaking effect between π and K meson, because the meson decay constant $f_\rho > f_K$. The penguin amplitude (P) for the $\bar{B} \to \pi^+\rho^-$ decay, even if with a larger decay constant, is smaller than the corresponding $\bar{B} \to \pi^+\pi^-$ decay, because there is no chiral enhanced penguin contribution for a vector meson emission shown in Eq. (4). If the emitted meson is a pseudoscalar scalar meson in $B \to VP$ decays, its difference from $B \to PP$ decays is the $B \to V$ transition form factor differing from the $B \to P$ transition form factor. For example, we have the following difference between two decay channels is $B \to \pi$ form factor and $B \to \rho$ form factor, which is smaller than the difference between the π

and the ρ decay constants:

$$|T(B^- \to \pi^0\pi^-)| : |T(B^- \to \rho^-\pi^0)| = 1 : 1.24, \quad (44)$$

$$|C(B^- \to \pi^0\pi^-)| : |C(B^- \to \rho^-\pi^0)| = 1 : 1.25, \quad (45)$$

$$|P(\bar{B}^0 \to \pi^+\pi^-)| : |P(\bar{B}^0 \to \rho^-\pi^+)| = 1 : 0.59, \quad (46)$$

$$|P_C(B^- \to \eta\pi^-)| : |P_C(B^- \to \rho^-\eta)| = 1 : 1.26. \quad (47)$$

The penguin amplitude (P) for the $\bar{B} \to \rho^-\pi^+$ decay, even if with a larger decay constant, is smaller than the corresponding $\bar{B} \to \pi^+\pi^-$ decay, because the chiral enhanced penguin contributions cancel some of the factorization penguin contribution by a minus sign, shown in Eq. (4). For decays induced by $b \to s$ transition, we have

$$|T(B^- \to \pi^0 K^-)| : |T(B^- \to \pi^0 K^{*-})| = 1 : 1.42, \quad (48)$$

$$|C(B^- \to \pi^0 K^-)| : |C(B^- \to K^{*-}\pi^0)| = 1 : 1.23, \quad (49)$$

$$|P(\bar{B}^0 \to \pi^+ K^-)| : |P(\bar{B}^0 \to \pi^+ K^{*-})| = 1 : 0.68, \quad (50)$$

$$|P_C(B^- \to \eta K^-)| : |P_C(B^- \to K^{*-}\eta)| = 1 : 1.24. \quad (51)$$

It is apparent that the difference characterized by the K and K^* decay constant is large.

4 Conclusion

In this paper, we studied two-body charmless hadronic B decays in a factorization-assisted topological-amplitude approach. Since factorization has been proven to all orders in α_s in the so-called soft-collinear effective theory at leading order in Λ/m_b expansion, the color-favored tree emission diagram T was factorized into short-distance effective Wilson coefficients and decay constants and form factors, without free parameters. The flavor $SU(3)$ breaking effects are then automatically considered in different meson decay constants and transition form factors. The factorization theorem is not proven in most other topological diagrams. They were considered as universal magnitudes (χ) and associated phases (ϕ) in the conventional flavor diagram approach to be fitted from the experimental data. In our approach, as regards the corresponding decay constants, the form factors were factorized out from them before the χ^2 fit assisted by a factorization hypothesis to indicate the flavor $SU(3)$ breaking effect. In addition to the large tree and QCD-penguin diagrams studied in these types of decays, the electroweak penguin contribution (P_{EW}) was also included, which is not negligible but essential for $B \to \pi K$ decays, especially for the CP asymmetry parameters. Unlike the previous conventional flavor diagram approach, this contribution was factorized into short-distance effective Wilson coefficients and decay constants and form factors, just like the color-favored tree emission diagram T.

There were six parameters, $\chi^C(\phi^C)$, $\chi^{C'}(\phi^{C'})$, and $\chi^E(\phi^E)$ for tree diagrams C, E and eight parameters $\chi^P(\phi^P)$, $\chi^{P_C}(\phi^{P_C})$, $\chi^{P'_C}(\phi^{P'_C})$, and $\chi^{P_A}(\phi^{P_A})$ for QCD-penguin diagrams to be fitted from 48 measured data of branching ratios and CP asymmetry parameters. Since $SU(3)$ breaking effects and the difference between pseudoscalar and vector meson have been already considered in the decay constants and form factors, we can fit all the $B \to PP, PV$ decays together. The number of free parameters is greatly reduced. These parameters were extracted precisely even for small parameters χ^E, ϕ^E, which had large uncertainties in the conventional flavor diagram approach. Besides, the χ^2 per degree of freedom is smaller than the conventional flavor diagram approach, even with much more free parameters in their approach. With the fitted parameters, we predicted branching fractions of $B_{(s)} \to PP, PV$ decay modes and their CP asymmetry parameters. The long-standing puzzles of $\pi\pi$ branching ratios and $\pi K CP$ asymmetry have been resolved consistently with not too large color-suppressed tree diagram contribution χ^C. For the B_s decays, we do not include any data as input in the χ^2 fit, but all as theoretical predictions, since very few channels have been measured. The flavor $SU(3)$ breaking effect between π and K were approximately 10%, even more than 20% in the ρ and K^* meson cases and larger in π and ρ, K, and K^*.

Acknowledgements We are grateful to Hsiang-nan Li, Wei Wang, Rui Zhou, Fusheng Yu, Ying Li, and Qin Qin for useful discussion. We also thank Fred James providing help for analyzing the error bar in the Minuit program. The work is partly supported by the National Science Foundation of China (11375208, 11521505, 11621131001 and 11235005).

References

1. A.J. Bevan et al. [BaBar and Belle Collaborations], Eur. Phys. J. C **74**, 3026 (2014). doi:10.1140/epjc/s10052-014-3026-9. arXiv:1406.6311 [hep-ex]
2. R. Aaij et al. [LHCb Collaboration], Eur. Phys. J. C **73**(4), 2373 (2013). doi:10.1140/epjc/s10052-013-2373-2. arXiv:1208.3355 [hep-ex]
3. M. Bauer, B. Stech, M. Wirbel, Z. Phys. C **34**, 103 (1987). doi:10.1007/BF01561122

4. A. Ali, G. Kramer, C.-D. Lu, Phys. Rev. D **58**, 094009 (1998). doi:10.1103/PhysRevD.58.094009. arXiv:hep-ph/9804363
5. A. Ali, G. Kramer, C.-D. Lu, Phys. Rev. D **59**, 014005 (1999). doi:10.1103/PhysRevD.59.014005. arXiv:hep-ph/9805403
6. M. Beneke, G. Buchalla, M. Neubert, C.T. Sachrajda, Nucl. Phys. B **591**, 313 (2000). doi:10.1016/S0550-3213(00)00559-9. arXiv:hep-ph/0006124
7. C.D. Lu, K. Ukai, M.Z. Yang, Phys. Rev. D **63**, 074009 (2001). doi:10.1103/PhysRevD.63.074009. arXiv:hep-ph/0004213
8. Y.Y. Keum, H.N. Li, A.I. Sanda, Phys. Rev. D **63**, 054008 (2001). doi:10.1103/PhysRevD.63.054008. arXiv:hep-ph/0004173
9. C.W. Bauer, S. Fleming, D. Pirjol, I.W. Stewart, Phys. Rev. D **63**, 114020 (2001). doi:10.1103/PhysRevD.63.114020. arXiv:hep-ph/0011336
10. H.Y. Cheng, C.K. Chua, Phys. Rev. D **80**, 114008 (2009). doi:10.1103/PhysRevD.80.114008. arXiv:0909.5229 [hep-ph]
11. C.W. Bauer, D. Pirjol, I.Z. Rothstein, I.W. Stewart, Phys. Rev. D **70**, 054015 (2004). doi:10.1103/PhysRevD.70.054015. arXiv:hep-ph/0401188
12. H.N. Li, S. Mishima, A.I. Sanda, Phys. Rev. D **72**, 114005 (2005). doi:10.1103/PhysRevD.72.114005. arXiv:hep-ph/0508041
13. H.N. Li, S. Mishima, Phys. Rev. D **90**(7), 074018 (2014). doi:10.1103/PhysRevD.90.074018. arXiv:1407.7647 [hep-ph]
14. Y.K. Hsiao, C.F. Chang, X.G. He, Phys. Rev. D **93**(11), 114002 (2016). doi:10.1103/PhysRevD.93.114002. arXiv:1512.09223 [hep-ph]
15. C.W. Chiang, Y.F. Zhou, J. High Energy Phys. **12**, 027 (2006)
16. C.W. Chiang, Y.F. Zhou, J. High Energy Phys. **03**, 055 (2009)
17. H.Y. Cheng, C.W. Chiang, A.L. Kuo, Phys. Rev. D **91**(1), 014011 (2015). doi:10.1103/PhysRevD.91.014011. arXiv:1409.5026 [hep-ph]
18. H.N. Li, C.D. Lu, F.S. Yu, Phys. Rev. D **86**, 036012 (2012). doi:10.1103/PhysRevD.86.036012. arXiv:1203.3120 [hep-ph]
19. H.N. Li, C.D. Lu, Q. Qin, F.S. Yu, Phys. Rev. D **89**(5), 054006 (2014). doi:10.1103/PhysRevD.89.054006. arXiv:1305.7021 [hep-ph]
20. Q. Qin, H.N. Li, C.D. Lü, F.S. Yu, Int. J. Mod. Phys. Conf. Ser. **29**, 1460209 (2014). doi:10.1142/S2010194514602099
21. R. Aaij et al. [LHCb Collaboration], Phys. Rev. Lett. **116**(19), 191601 (2016). doi:10.1103/PhysRevLett.116.191601. arXiv:1602.03160 [hep-ex]
22. S.H. Zhou, Y.B. Wei, Q. Qin, Y. Li, F.S. Yu, C.D. Lu, Phys. Rev. D **92**(9), 094016 (2015). doi:10.1103/PhysRevD.92.094016. arXiv:1509.04060 [hep-ph]
23. M. Ciuchini, E. Franco, G. Martinelli, M. Pierini, L. Silvestrini, Phys. Lett. B **674**, 197 (2009). doi:10.1016/j.physletb.2009.03.011. arXiv:0811.0341 [hep-ph]
24. M. Beneke, T. Huber, X.Q. Li, Nucl. Phys. B **832**, 109 (2010). doi:10.1016/j.nuclphysb.2010.02.002. arXiv:0911.3655 [hep-ph]
25. W. Wang, Y.M. Wang, D.S. Yang, C.D. Lu, Phys. Rev. D **78**, 034011 (2008). doi:10.1103/PhysRevD.78.034011. arXiv:0801.3123 [hep-ph]
26. K.A. Olive et al. [Particle Data Group Collaboration], Chin. Phys. C **38**, 090001 (2014). doi:10.1088/1674-1137/38/9/090001
27. M. Beneke, M. Neubert, Nucl. Phys. B **675**, 333 (2003). doi:10.1016/j.nuclphysb.2003.09.026. arXiv:hep-ph/0308039
28. M. Beneke, G. Buchalla, M. Neubert, C.T. Sachrajda, Nucl. Phys. B **606**, 245 (2001). doi:10.1016/S0550-3213(01)00251-6. arXiv:hep-ph/0104110
29. Z. Rui, G. Xiangdong, C.D. Lu, Eur. Phys. J. C **72**, 1923 (2012). doi:10.1140/epjc/s10052-012-1923-3. arXiv:1111.0181 [hep-ph]
30. H.Y. Cheng, C.K. Chua, C.W. Hwang, Phys. Rev. D **69**, 074025 (2004). doi:10.1103/PhysRevD.69.074025. arXiv:hep-ph/0310359
31. P. Ball, G.W. Jones, R. Zwicky, Phys. Rev. D **75**, 054004 (2007). doi:10.1103/PhysRevD.75.054004. arXiv:hep-ph/0612081
32. A. Bharucha, D.M. Straub, R. Zwicky, arXiv:1503.05534 [hep-ph]
33. M. Jamin, B.O. Lange, Phys. Rev. D **65**, 056005 (2002). doi:10.1103/PhysRevD.65.056005
34. P. Gelhausen, A. Khodjamirian, A.A. Pivovarov, D. Rosenthal, Phys. Rev. D **88**, 014015 (2013). Erratum: [Phys. Rev. D **89**, 099901 (2014)]. Erratum: [Phys. Rev. D **91**, 099901 (2015)]. doi:10.1103/PhysRevD.88.014015, 10.1103/PhysRevD.91.099901, 10.1103/PhysRevD.89.099901. arXiv:1305.5432 [hep-ph]
35. A.A. Penin, M. Steinhauser, Phys. Rev. D **65**, 054006 (2002). doi:10.1103/PhysRevD.65.054006. arXiv:hep-ph/0108110
36. S. Narison, Phys. Lett. B **520**, 115 (2001). doi:10.1016/S0370-2693(01)01116-9. arXiv:hep-ph/0108242
37. W. Lucha, D. Melikhov, S. Simula, J. Phys. G **38**, 105002 (2011). doi:10.1088/0954-3899/38/10/105002. arXiv:1008.2698 [hep-ph]
38. S. Narison, Phys. Lett. B **718**, 1321 (2013). doi:10.1016/j.physletb.2012.10.057. arXiv:1209.2023 [hep-ph]
39. R.J. Dowdall et al. [HPQCD Collaboration], Phys. Rev. Lett. **110**(22), 222003 (2013). doi:10.1103/PhysRevLett.110.222003. arXiv:1302.2644 [hep-lat]
40. N. Carrasco et al., PoS LATTICE **2013**, 313 (2014). arXiv:1311.2837 [hep-lat]
41. P. Dimopoulos et al. [ETM Collaboration], JHEP **1201**, 046 (2012). doi:10.1007/JHEP01(2012)046. arXiv:1107.1441 [hep-lat]
42. C. McNeile, C.T.H. Davies, E. Follana, K. Hornbostel, G.P. Lepage, Phys. Rev. D **85**, 031503 (2012). doi:10.1103/PhysRevD.85.031503. arXiv:1110.4510 [hep-lat]
43. A. Bazavov et al. [Fermilab Lattice and MILC Collaborations], Phys. Rev. D **85**, 114506 (2012). doi:10.1103/PhysRevD.85.114506. arXiv:1112.3051 [hep-lat]
44. H. Na, C.J. Monahan, C.T.H. Davies, R. Horgan, G.P. Lepage, J. Shigemitsu, Phys. Rev. D **86**, 034506 (2012). doi:10.1103/PhysRevD.86.034506. arXiv:1202.4914 [hep-lat]
45. A. Bussone et al., arXiv:1411.5566 [hep-lat]
46. F. Bernardoni et al. [ALPHA Collaboration], Phys. Lett. B **735**, 349 (2014). doi:10.1016/j.physletb.2014.06.051. arXiv:1404.3590 [hep-lat]
47. D. Melikhov, B. Stech, Phys. Rev. D **62**, 014006 (2000). doi:10.1103/PhysRevD.62.014006. arXiv:hep-ph/0001113
48. C.Q. Geng, C.W. Hwang, C.C. Lih, W.M. Zhang, Phys. Rev. D **64**, 114024 (2001). doi:10.1103/PhysRevD.64.114024. arXiv:hep-ph/0107012
49. C.D. Lu, W. Wang, Z.T. Wei, Phys. Rev. D **76**, 014013 (2007). doi:10.1103/PhysRevD.76.014013. arXiv:hep-ph/0701265
50. C. Albertus, Phys. Rev. D **89**(6), 065042 (2014). doi:10.1103/PhysRevD.89.065042. arXiv:1401.1791 [hep-ph]
51. H.Y. Cheng, C.K. Chua, Phys. Rev. D **81**, 114006 (2010). Erratum: [Phys. Rev. D **82**, 059904 (2010)]. doi:10.1103/PhysRevD.81.114006, 10.1103/PhysRevD.82.059904. arXiv:0909.4627 [hep-ph]
52. C.H. Chen, Y.L. Shen, W. Wang, Phys. Lett. B **686**, 118 (2010). doi:10.1016/j.physletb.2010.02.056. arXiv:0911.2875 [hep-ph]
53. P. Ball, V.M. Braun, Phys. Rev. D **58**, 094016 (1998). doi:10.1103/PhysRevD.58.094016. arXiv:hep-ph/9805422
54. P. Ball, JHEP **9809**, 005 (1998). doi:10.1088/1126-6708/1998/09/005. arXiv:hep-ph/9802394
55. P. Ball, R. Zwicky, JHEP **0110**, 019 (2001). doi:10.1088/1126-6708/2001/10/019. arXiv:hep-ph/0110115
56. P. Ball, R. Zwicky, Phys. Rev. D **71**, 014015 (2005). doi:10.1103/PhysRevD.71.014015. arXiv:hep-ph/0406232
57. P. Ball, R. Zwicky, Phys. Rev. D **71**, 014029 (2005). doi:10.1103/PhysRevD.71.014029. arXiv:hep-ph/0412079
58. P. Ball, G.W. Jones, JHEP **0708**, 025 (2007). doi:10.1088/1126-6708/2007/08/025. arXiv:0706.3628 [hep-ph]
59. J. Charles, A. Le Yaouanc, L. Oliver, O. Pene, J.C. Raynal, Phys. Rev. D **60**, 014001 (1999). doi:10.1103/PhysRevD.60.014001. arXiv:hep-ph/9812358

60. A. Bharucha, T. Feldmann, M. Wick, JHEP **1009**, 090 (2010). doi:10.1007/JHEP09(2010)090. arXiv:1004.3249 [hep-ph]
61. A. Bharucha, JHEP **1205**, 092 (2012). doi:10.1007/JHEP05(2012)092. arXiv:1203.1359 [hep-ph]
62. A. Khodjamirian, T. Mannel, N. Offen, Phys. Rev. D **75**, 054013 (2007). doi:10.1103/PhysRevD.75.054013. arXiv:hep-ph/0611193
63. A. Khodjamirian, T. Mannel, N. Offen, Y.-M. Wang, Phys. Rev. D **83**, 094031 (2011). doi:10.1103/PhysRevD.83.094031. arXiv:1103.2655 [hep-ph]
64. Y.M. Wang, Y.L. Shen, Nucl. Phys. B **898**, 563 (2015). doi:10.1016/j.nuclphysb.2015.07.016. arXiv:1506.00667 [hep-ph]
65. U.G. Meissner, W. Wang, Phys. Lett. B **730**, 336 (2014). doi:10.1016/j.physletb.2014.02.009. arXiv:1312.3087 [hep-ph]
66. Y.L. Wu, M. Zhong, Y.B. Zuo, Int. J. Mod. Phys. A **21**, 6125 (2006). doi:10.1142/S0217751X06033209. arXiv:hep-ph/0604007
67. X.G. Wu, T. Huang, Phys. Rev. D **79**, 034013 (2009). doi:10.1103/PhysRevD.79.034013. arXiv:0901.2636 [hep-ph]
68. G. Duplancic, A. Khodjamirian, T. Mannel, B. Melic, N. Offen, JHEP **0804**, 014 (2008). doi:10.1088/1126-6708/2008/04/014. arXiv:0801.1796 [hep-ph]
69. M.A. Ivanov, J.G. Korner, S.G. Kovalenko, P. Santorelli, G.G. Saidullaeva, Phys. Rev. D **85**, 034004 (2012). doi:10.1103/PhysRevD.85.034004. arXiv:1112.3536 [hep-ph]
70. M. Ahmady, R. Campbell, S. Lord, R. Sandapen, Phys. Rev. D **89**(7), 074021 (2014). doi:10.1103/PhysRevD.89.074021. arXiv:1401.6707 [hep-ph]
71. H.B. Fu, X.G. Wu, Y. Ma, J. Phys. G **43**(1), 015002 (2016). doi:10.1088/0954-3899/43/1/015002. arXiv:1411.6423 [hep-ph]
72. H.N. Li, Y.L. Shen, Y.M. Wang, Phys. Rev. D **85**, 074004 (2012). doi:10.1103/PhysRevD.85.074004. arXiv:1201.5066 [hep-ph]
73. W.F. Wang, Z.J. Xiao, Phys. Rev. D **86**, 114025 (2012). doi:10.1103/PhysRevD.86.114025. arXiv:1207.0265 [hep-ph]
74. W.F. Wang, Y.Y. Fan, M. Liu, Z.J. Xiao, Phys. Rev. D **87**(9), 097501 (2013). doi:10.1103/PhysRevD.87.097501. arXiv:1301.0197
75. Y.Y. Fan, W.F. Wang, S. Cheng, Z.J. Xiao, Chin. Sci. Bull. **59**, 125 (2014). doi:10.1007/s11434-013-0049-9. arXiv:1301.6246 [hep-ph]
76. Y.Y. Fan, W.F. Wang, Z.J. Xiao, Phys. Rev. D **89**(1), 014030 (2014). doi:10.1103/PhysRevD.89.014030. arXiv:1311.4965 [hep-ph]
77. T. Kurimoto, H.N. Li, A.I. Sanda, Phys. Rev. D **65**, 014007 (2002). doi:10.1103/PhysRevD.65.014007. arXiv:hep-ph/0105003
78. C.D. Lu, M.Z. Yang, Eur. Phys. J. C **28**, 515 (2003). doi:10.1140/epjc/s2003-01199-y. arXiv:hep-ph/0212373
79. Z.T. Wei, M.Z. Yang, Nucl. Phys. B **642**, 263 (2002). doi:10.1016/S0550-3213(02)00623-5. arXiv:hep-ph/0202018
80. T. Huang, X.G. Wu, Phys. Rev. D **71**, 034018 (2005). doi:10.1103/PhysRevD.71.034018. arXiv:hep-ph/0412417
81. R.R. Horgan, Z. Liu, S. Meinel, M. Wingate, Phys. Rev. D **89**(9), 094501 (2014). doi:10.1103/PhysRevD.89.094501. arXiv:1310.3722 [hep-lat]
82. E. Dalgic, A. Gray, M. Wingate, C.T.H. Davies, G.P. Lepage, J. Shigemitsu, Phys. Rev. D **73**, 074502 (2006). Erratum: [Phys. Rev. D **75**, 119906 (2007)]. doi:10.1103/PhysRevD.75.119906, 10.1103/PhysRevD.73.074502. arXiv:hep-lat/0601021
83. S. Aoki et al., Eur. Phys. J. C **74**, 2890 (2014). doi:10.1140/epjc/s10052-014-2890-7. arXiv:1310.8555 [hep-lat]
84. F. Ambrosino et al., JHEP **0907**, 105 (2009). doi:10.1088/1126-6708/2009/07/105. arXiv:0906.3819 [hep-ph]
85. T. Feldmann, P. Kroll, B. Stech, Phys. Rev. D **58**, 114006 (1998). doi:10.1103/PhysRevD.58.114006. arXiv:hep-ph/9802409
86. T. Feldmann, P. Kroll, B. Stech, Phys. Lett. B **449**, 339 (1999). doi:10.1016/S0370-2693(99)00085-4. arXiv:hep-ph/9812269
87. F. James, M. Winker, http://www.cern.ch/minuit. CERN, May 2004
88. Y. Li, C.D. Lu, Z.J. Xiao, X.Q. Yu, Phys. Rev. D **70**, 034009 (2004). doi:10.1103/PhysRevD.70.034009. arXiv:hep-ph/0404028
89. A. Ali, G. Kramer, Y. Li, C.D. Lu, Y.L. Shen, W. Wang, Y.M. Wang, Phys. Rev. D **76**, 074018 (2007). doi:10.1103/PhysRevD.76.074018. arXiv:hep-ph/0703162
90. Z.J. Xiao, W.F. Wang, Y.Y. Fan, Phys. Rev. D **85**, 094003 (2012). doi:10.1103/PhysRevD.85.094003. arXiv:1111.6264 [hep-ph]